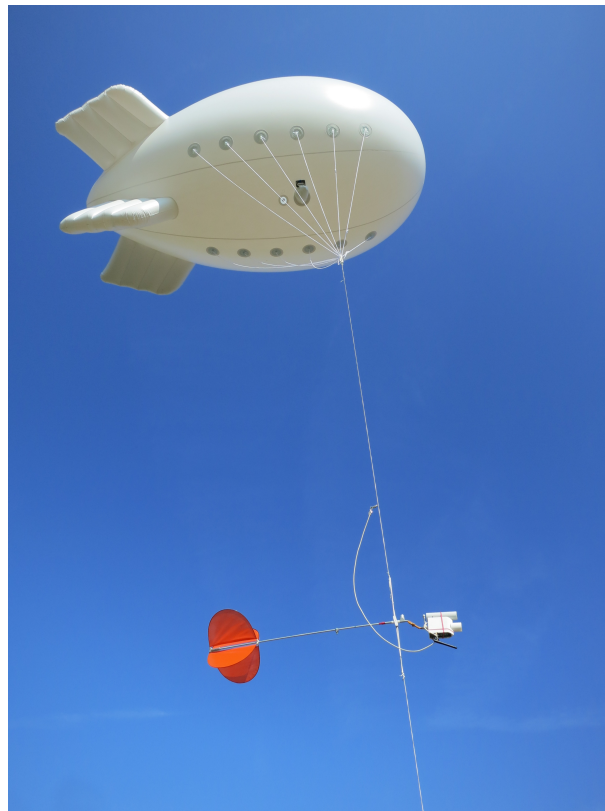


BACHELOR THESIS

Observation of the lower atmospheric boundary layer with fiber optic distributed sensing

Antonia Fritz



Supervision

Dr. Karl Lapo

Prof. Dr. Christoph Thomas

Declaration of Authorship

I herewith certify that the work presented below with the title " Observation of the lower atmospheric boundary layer with fiber optic distributed sensing" is to the best of my knowledge and belief original and the result of my own investigations. Third party work, non-published and published information I received are properly and duly acknowledged. This work has never previously been submitted to any other examination committee.

Place, Date: _____

Antonia Fritz: _____

Acknowledgement

Many thanks to Karl and Christoph, who were great supervisors during the entire project. Without Christoph FlyFox probably would never have flown and I certainly would have needed much longer for all the preparatory steps without his help and advice. Karl especially converted my raw data into temperature data and supported me a lot in data analysis and interpretation. Thanks for that and for all the tea/coffee during our sometimes really long discussions!

Thanks also to Anita, Andreas, Karl, Christoph and Nico for staying overnight with me in Voitsumra and for launching the balloon together. That would not have been possible alone, so thank you for even getting up with me at 4 o'clock.

Furthermore, I want to thank Johann and Jo for all their technical support, for teaching me to solder and for building the tether sonde with / for me. Also, thanks to Lena for printing (several iterations of) the tether sonde casings - the DarkMix logo looks great on them now!

Contents

| | |
|---|------------|
| Declaration of Authorship | i |
| Acknowledgement | ii |
| Table of Content | iii |
| List of Figures | v |
| Zusammenfassung | 1 |
| Abstract | 1 |
| 1 Introduction | 2 |
| 1.1 The Atmospheric Boundary Layer | 2 |
| 1.2 The DarkMix project | 3 |
| 1.3 The FlyFox-V experiment | 3 |
| 2 Research questions and hypothesis | 4 |
| 3 Experimental site | 5 |
| 4 Material | 5 |
| 4.1 Theory of Fiber Optic Distributed Sensing | 5 |
| 4.2 Installation of FODS at the FlyFox-V | 6 |
| 4.3 Specification of FlyFox-V material and instruments | 8 |
| 4.3.1 Tethered balloon and safety deflation device | 8 |
| 4.3.2 Tether sonde | 9 |
| 4.3.3 Reference baths | 10 |
| 4.3.4 DTS device | 11 |
| 4.3.5 Further material | 11 |
| 4.4 LiDAR | 11 |
| 5 Methods | 11 |
| 5.1 Process of launching the FlyFox-V | 11 |
| 5.2 Processing of the DTS data | 12 |
| 5.3 Response of the balloon to the changing meteorological conditions | 12 |
| 5.4 Method for the LAF to height conversion | 13 |
| 5.4.1 Uncertainty of the flying height | 14 |
| 5.4.2 Linear approximation | 14 |
| 5.4.3 Parabolic approximation | 15 |
| 5.4.4 Catenary approximation | 17 |
| 5.4.5 Comparison of approximations | 17 |
| 5.5 Investigation of the stable boundary layer | 17 |
| 5.5.1 Influence of height approximations | 18 |
| 5.5.2 The morning transition | 19 |
| 5.5.3 Bottom-up approach | 19 |

| | | |
|----------|--|-----------|
| 6 | Results and Interpretation | 20 |
| 6.1 | Evaluation of the experimental set-up | 20 |
| 6.2 | Response of the balloon to changing conditions | 20 |
| 6.3 | LAF to height conversion | 22 |
| 6.3.1 | Calculated parameters of the approximations | 22 |
| 6.3.2 | Comparison of approximations | 22 |
| 6.3.3 | Interpretation of the LAF to height conversion | 25 |
| 6.4 | Temperature profiles of the lower ABL | 27 |
| 6.5 | Investigation of the stable boundary layer | 29 |
| 6.5.1 | Influence of height approximation | 29 |
| 6.5.2 | The morning transition | 31 |
| 6.5.3 | Morning transition phase on the 18 th of July | 36 |
| 6.5.4 | Bottom-up approach | 37 |
| 7 | Conclusion | 43 |
| A | List of Material | 45 |
| B | FlyFox-V Check-lists | 47 |
| B.1 | Refill Check-list | 47 |
| B.2 | Preparation Check-list | 48 |
| B.3 | Launching Check-list | 50 |
| B.4 | Take down Check-list | 52 |
| C | Documentation forms | 54 |

List of Figures

| | | |
|----|---|----|
| 1 | Daily evolution of the atmospheric boundary layer | 2 |
| 2 | Location of the FlyFox-V launching area | 6 |
| 3 | Sketch of the FlyFox-V set-up | 7 |
| 4 | FlyFox-V launching area during a morning flight | 8 |
| 5 | The balloon when fixed on the ground | 8 |
| 6 | Outlets of the tethered balloon | 9 |
| 7 | Tether sonde | 10 |
| 8 | Reference baths during a flight | 10 |
| 9 | Schema of fiber bend | 13 |
| 10 | Schema of linear height approximation | 14 |
| 11 | Correlation of horizontal wind speed and height offset from 200 m | 21 |
| 12 | Correlation of vertical wind speed and height change since the previous measurement | 22 |
| 13 | Comparison of the three height approximations for $\alpha = 10^\circ$ | 24 |
| 14 | Comparison of the three height approximations for $\alpha = 15^\circ$ | 24 |
| 15 | Comparison of the three height approximations for $\alpha = 22.6^\circ$ | 25 |
| 16 | Profile of potential temperature on the 18 th of July | 27 |
| 17 | Profile of potential temperature on the 22 nd of July | 28 |
| 18 | Profile of potential temperature on the 23 rd of July | 28 |
| 19 | Profile of potential temperature on the 26 th of July | 29 |
| 20 | Difference between gradients calculated with the linear and the parabolic height approximation | 30 |
| 21 | Smoothed gradients of potential temperatures with linearly and parabolic approximated heights | 30 |
| 22 | Sensible heat flux (solid line), MT (dashed line), and sunrise (dotted line) . | 31 |
| 23 | Horizontal wind speeds measured by the CSAT in 1.25 m a.g.l. (solid line) and MT (dashed line) | 32 |
| 24 | $\frac{\delta\theta}{\delta z}$ -profile of the 18 th of July, sunrise (dotted line) and MT (dashed line) . . | 33 |
| 25 | $\frac{\delta\theta}{\delta z}$ -profile of the 22 nd of July, sunrise (dotted line), MT (dashed line) and SBL boundaries (solid line) | 33 |
| 26 | $\frac{\delta\theta}{\delta z}$ -profile of the 23 rd of July, sunrise (dotted line), MT (dashed line) and SBL boundaries (solid line) | 34 |
| 27 | $\frac{\delta\theta}{\delta z}$ -profile of the 26 th of July, sunrise (dotted line), MT (dashed line) and SBL boundaries (solid line) | 34 |
| 28 | Fog layer on the 18 th of July, 2019 | 37 |
| 29 | Comparison of initial conditions for all morning transitions | 38 |
| 30 | Visualization of the Internal Layers 1, 2, and 3 | 39 |
| 31 | CSAT wind speed data with highlighted strong stable layers (darkblue) and weak stable layer (lightblue), 22 nd of July | 40 |
| 32 | CSAT flux and temperature data with highlighted strong stable layers (darkblue) and weak stable layer (lightblue), 22 nd of July | 41 |
| 33 | Wind direction for the 22 nd of July with highlighted strong stable layers (darkblue) and weak stable layer (lightblue) | 42 |
| 34 | Flight sheet of the 18.07.2019 | 55 |
| 35 | Flight sheet of the 22.07.2019 | 56 |
| 36 | Flight sheet of the 23.07.2019 | 57 |

| | | |
|----|--|----|
| 37 | Flight sheet of the 26.07.2019 | 58 |
|----|--|----|

Zusammenfassung

Die untere atmosphärische Grenzschicht wird mit der neuen Technik des "Fiber Optic Distributed Sensing" an einem Heliumballon untersucht. Die gemessenen Temperaturprofile zeigen, dass die Transformation von der nächtlich stabilen Grenzschicht zur tageszeitlichen turbulent gemischten Grenzschicht ein langer und nicht ausschließlich von Oberflächenprozessen angetriebener Prozess ist.

Die Messungen des FlyFox-V Experiments liefern Temperaturprofile der bodennahen 200 m mit einer zeitlichen Auflösung von 10 s und einer räumlichen Auflösung von 25 cm. Sie werden in einem weiten Tal im Norden Bayerns, Deutschland, durchgeführt. Es werden vier Messungen der Morgenstunden zwischen 5:00 und 8:30 Uhr (Ortszeit) analysiert. Diese Messungen zeigen, dass die Morgen-Transformation ein Prozess mit variierender zeitlicher und räumlicher Ausdehnung ist. Darüber hinaus ist ersichtlich, dass sich die Morgen-Transformation aus zwei gleichbedeutenden Teil-Transformationen zusammensetzt: eine an der oberen und eine an der unteren Grenze der stabilen Grenzschicht. Da während des untersuchten Messzeitraums zudem eine Entkopplung zwischen aneinandergrenzenden oberflächennahen Luftschichten erkennbar ist, kann die Morgen-Transformation und die Bewegung zusammenhängender Luftmassen innerhalb der stabilen Grenzschicht nicht rein durch Oberflächenprozesse erklärt werden.

Abstract

The lower atmospheric boundary layer is observed with the new technique of fiber optic distributed sensing on a tethered balloon. The gained temperature profiles reveal that the transformation from the nocturnal stable boundary layer to the daytime mixed boundary layer is a long process and not solely driven by surface processes.

The measurements of the FlyFox-V experiment provide temperature profiles from the surface up to 200 m with a time resolution of 10 s and a spatial resolution of 25 cm. They are conducted in a broad mountain valley in northern Bavaria, Germany. Four measurements of the morning hours between 5:00 am and 8:30 am (local time) are analyzed. The measurements show that the morning transition is a process with varying temporal and spatial extent. Furthermore, they show that the transformation occurs simultaneously at the top and bottom boundary of the stable boundary layer. These two separate transformations at the two boundaries are equally important for the overall transition of the stable boundary layer. In addition, for the observed measurement, a decoupling between adjoining near-surface air layers is found. Hence, the morning transition and the movement of internal layers within the stable boundary layer cannot be explained by surface processes during the investigated time interval.

1 Introduction

1.1 The Atmospheric Boundary Layer

As humans we constantly breathe the air of the atmosphere from which we can taste salt if we're near an ocean or smell the flowers if we're passing a wildflower meadow. These experiences demonstrate that this lowest part of the atmosphere we're living in is directly influenced by the earth's surface. In this layer of the atmosphere important processes such as evapotranspiration, heat transfer, or CO_2 transport take place and the flows get modified by the topography and surface friction. Therefore, this lowest part which reaches magnitudes between 100 and 3000 m is called the **A**tmospheric **B**oundary **L**ayer (ABL).

The ABL is not a temporally and spatially uniform volume of air but evolves during a diurnal cycle as visualized in Figure 1:

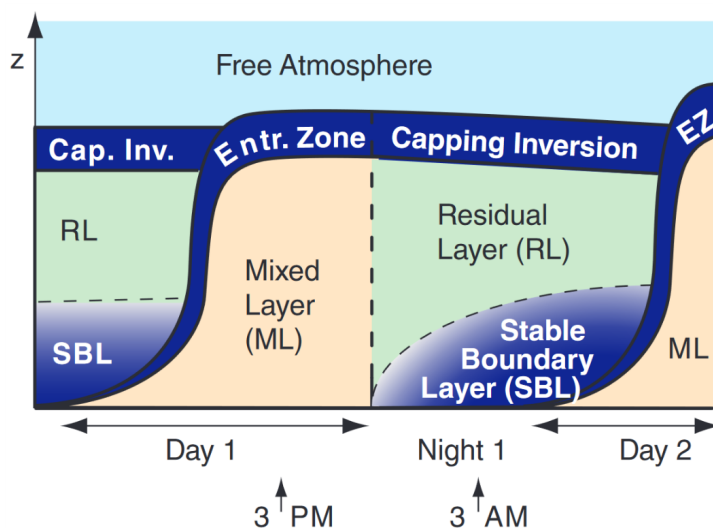


Figure 1: Daily evolution of the atmospheric boundary layer [7]

In the morning, when the sun rises, the downwelling shortwave radiation from the sun increases rapidly and the surface heats up. This heating leads to strong buoyancy forces which are directed upwards and therefore are defined as positive. The stratification becomes unstable and a convectively driven development of a turbulent **Mixed Layer (ML)** starts. The magnitude of this ML increases with increasing heating. At its top the ML is connected to the free atmosphere by a so called entrainment zone, in which less turbulent air is mixed into the ABL.

As the sun sets the shortwave radiation vanishes. The longwave emission of the surface dominates leading to a cooling of the ground and the air close to it. The sign of the buoyancy forces turns to negative, which means they are directed towards the surface. Due to the negative buoyancy forces stable stratification and a **Stable Boundary Layer (SBL)** develops. The higher part of the former ML then forms a **Residual Layer (RL)**, which is usually neutrally stratified and where the turbulence is nearly equal in all directions. Above the RL a capping inversion covers the ABL and prevents exchange between the ABL and the free atmosphere.

During the entire day a surface layer can be defined. It is the lowest part of the ABL in which turbulent fluxes and stress vary by less than 10% of their magnitude [8].

1.2 The DarkMix project

The DarkMix project aims to understand how the ABL behaves in the SBL, particularly on a submeso-scale under stable, weak-wind conditions.

It is important to reach this goal as most weather and climate models are based on the concept of dynamic stability and assume turbulence to vanish under strong stability. However, observations confirm that weak, but finite turbulence occurs under strongly stable conditions and influences transport and mixing processes. This discrepancy between models and reality causes unrealistic model outputs and leads to the need of a better physical and conceptual understanding of the mechanisms that drive turbulence under strong stability and correspondingly under weak-wind conditions.

The DarkMix team aims to reach their goal of precisely understanding the behavior of the ABL by observing temperature and flow profiles. In the first phase of the project the focus laid on the technological innovations needed to make a distributed flow sensor possible by developing a fully 3-dimensional spatially distributed sensor of atmospheric flows using fiber optic distributed sensing (see Section 4.1 for details). In the second phase the new measuring technique is used to observe in-situ near-surface transport and mixing in three different landscapes: at a grassland near the village Voitsumra, at the forest of Waldstein Mountain, and in the city of Münster. The experiment of this bachelor thesis takes place at the first site and is part of the so called **Large Eddy Observatory Voitsumra Experiment (LOVE)**. The third phase of the DarkMix project is going to be the comparison of the observations gained in the field with the data gained from Large Eddy Simulations with the goal of detecting potential forcing mechanisms for the weak-wind turbulence. In the fourth and last phase the team will try to put all the information gained in the previous phases together in a new theoretical framework.

1.3 The FlyFox-V experiment

Within the broader research of DarkMix, this Bachelor thesis will analyze the lower part of the ABL in the sub-project called **Flying Fiber Optics Voitsumra (FlyFox-V)**. As in most parts of the LOVE project, the measuring technique is the **Fibre Optic Distributed Sensing (FODS)** method. The temperature is measured along an optical fiber (see Section 4 for a precise explanation) which with the help of a tethered balloon spans from the ground up to a height of about 200 m. Compared to traditional observation techniques, the FODS method has finer spatial (0.12 - 0.25 m) and temporal (1 - 10 s) resolution. Furthermore, it measures at a high accuracy. The temperature accuracy of FODS is up to 0.02 °C [10] and therefore much more precise than the accuracy of a SoDAR RASS (SoDAR PCS.2000 with RASS 1290 MHz, Metek GmbH, Elmshorn, Germany) with ≤ 0.3 °C [5]. However, FODS is a new technique, which makes it more difficult to deploy than typical observation systems. Additionally, it is limited in height as the fiber needs to stay connected to the ground.

The primary measuring time with FlyFox-V is in the morning as well as during the late afternoon or early evening as the transitions between the SBL and the MBL occur then. Calm, clear nights were preferred and the month July was chosen as it is known for weak-wind conditions at the experimental site.

The experiment is important for the whole LOVE project as it connects the observations taken with the near-surface observational network (0 - 12 m height) with traditional observations taken with a SoDAR RASS (20 - 240 m height), a LiDAR (0.25 - 5 km height), and a Ceilometer (0.18 - 7 km height). This presents the possibility of observing

the ABL along a vertical span of a few kilometers with very detailed profiles of wind speed (SoDAR RASS, LiDAR) and temperature (FlyFox-V, SoDAR RASS) at known cloud levels (Ceilometer), which is a novel observational breakthrough.

2 Research questions and hypothesis

This thesis is subdivided into an instrumental, technical part and a scientific, meteorological part. The first part is a necessary step to evaluate the whole process of data collection and to prepare the data for its meteorological analysis and interpretation. In this section, three main research topics are pursued:

1. The experimental setup and the process of data collection will be evaluated and suggestions for improvements will be developed.
2. The response of the balloon to changing meteorological conditions will be analyzed. The hypothesis is that the horizontal wind speeds have the greatest influence on the balloon's movement while vertical wind speeds and solar radiation play a subordinate role.
3. The length along the fiber optic cable of each measurement will be converted to a height value and the best approximation for this height will be determined. It is hypothesized that a linear height approximation is needed for calm situations and that a non-linear height approximation is needed for windy situations.

The first topic is of mainly practical use as its goal is to improve the data collection with FODS on a tethered balloon in general. During the flight as well as during the data analysis, the whole process was critically reviewed and all suggestions for improvements were summarized.

For the second research question, the influence of meteorological parameters on the balloon's movement was investigated. It was expected that the three parameters horizontal wind speed, vertical wind speed and solar radiation influence the flying height as the winds push the balloon in a particular direction and the radiation heats up the gas inside the balloon. From these three parameters, the horizontal wind speed was expected to have the greatest influence as it is much stronger than the vertical wind at the experimental site.

The third topic results from the need of a height value for each temperature measurement to interpret the data as temperature profiles. These height values are not provided by the DTS instrument which only returns the position of a measurement as its **L**ength **A**long the **F**iber (LAF). It was expected that two different height approximations are needed for the calm and the windy conditions as the course of the fiber looks clearly different during these conditions. Hence, a linear and two different non-linear height approximations are tested.

Once these methodological preparatory tasks have been accomplished, the second part of this thesis addresses the following two research questions:

1. Does the **M**orning **T**ransition (MT) observed by the traditional surface observations match the MT observed by FlyFox-V?
2. Is the occurrence and movement of distinct air layers induced by surface processes?

The MT can be defined as the first moment when the sensible heat flux (H) changes its sign in the morning [3]. This time is then used to specify when the SBL starts to turn neutral or unstable from below. There were three expectations about the MT: First, it was expected that H was negative during the night, which means its directed towards the surface and turns to positive after the MT. Second, it was expected that the MT would occur more than 2 h after sunrise. Different studies pointed out that in a flat terrain the MT would occur 1.3 h [1] or 2 h [3] after sunrise. For the FlyFox-V experiment in the valley, it was expected that the MT would occur later due to the shading of the surrounding mountains which delays the actual sunrise at the experimental site. Third, it was expected that the MT would occur later during days with stronger winds than during stays with calm conditions [3]. In the next step the data gained by traditional surface observations (CSAT sonic anemometers) and the data gained by the FlyFox-V experiment are compared. It was expected that the time of the MT (from CSAT data) and the moment when the stability of the near surface boundary layer changes from stable to neutral or unstable (from FlyFox-V data) are identical.

To answer the second research question, clearly distinguishable internal layers inside the stable boundary layer are selected from the FlyFox-V data. For the time of their occurrence, the wind speeds, wind direction, temperature, buoyancy flux, and momentum flux are investigated. It was expected that for each variable similar features occur throughout the different observed heights. Furthermore, it was expected that there is a time lag between a feature appearing close to the surface and the same feature appearing in greater heights. Due to this, it is expected that the occurrence of the internal layers visible in the FlyFox-V data can be explained by surface processes.

3 Experimental site

The LOVE experiment took place about 35 km from Bayreuth near the village Voitsumra in the district Wunsiedel in the northeastern part of Bavaria, Germany. The site is a multi-annual, agriculturally used grassland in the bottom of a broad valley in the Fichtelgebirge mountains. The elevation is 624 m above sea level.

The exact location of the FlyFox-V experiment within the large area of the LOVE project can be seen in Figure 2. Most of the LOVE project was located within the field marked orange being surrounded by a fence-like structure of horizontally deployed optical fiber. The FlyFox-V experiment took place outside of this main research area in the south western corner of the experimental site as marked with the red dot.

4 Material

4.1 Theory of Fiber Optic Distributed Sensing

As the traditional atmospheric observations work with single point measurements it is a common problem that the spatial extent of turbulent eddies can't be measured directly. To get around this problem Taylor's hypothesis is a commonly accepted theory [9]. It assumes that changes in single-point measurements are due to an unchanged pattern of eddies which moves with the advective wind. Furthermore it is assumed that eddies can be seen as frozen during the time they pass the sensor. Because of this hypothesis a long term but single-point observation is assumed to be equal to a short snapshot of all eddies



Figure 2: Location of the FlyFox-V launching area

in a large area if homogeneous and stationary conditions are given. This relationship is called ergodicity.

With the new FODS technique, spatially-distributed measurements of air temperature can now be taken at the same time. This improvement is especially important as Taylor's hypothesis does not hold under weak-wind conditions [6]. Furthermore, this technique doesn't need the assumptions of homogeneity and ergodicity.

The basic concept of FODS is that a laser impulse is sent through an optical fiber and its back scatter is measured. The ratio of the back-scattered stokes to anti-stokes frequency shifts depends on the temperature. Therefore, the temperature T at a time step t and a distance x from the instrument can be expressed as:

$$T(x, t) = \frac{\gamma}{\ln\left(\frac{P_S(x, t)}{P_{AS}(x, t)}\right) + C(t) - \int_0^x \Delta\alpha(x') dx'} \quad (1)$$

Here γ is a system specific constant of the unit K which represents the shift in energy between a photon at the laser wavelength and a photon which is scattered back. $P_S(x, t)$ and $P_{AS}(x, t)$ stand for the power of the stokes and anti-stokes frequencies, respectively. $C(t)$ is a calibration parameter which is defined by the instrument and the laser used. The integral expresses the differential attenuation of the stokes and anti-stokes photons within the optical fiber [10].

These three unknown parameters lead to the need of three reference sections along the optical fiber to enable a temperature calculation with Equation 1.

4.2 Installation of FODS at the FlyFox-V

This section explains the general setup of the experiment while Section 4.3 gives additional, more detailed information about the used material, the instruments and their purpose.

During FlyFox-V only passive FODS was used which means the optical fiber was not heated and thus only the temperature was measured. The experimental setup is shown schematically in Figure 3.

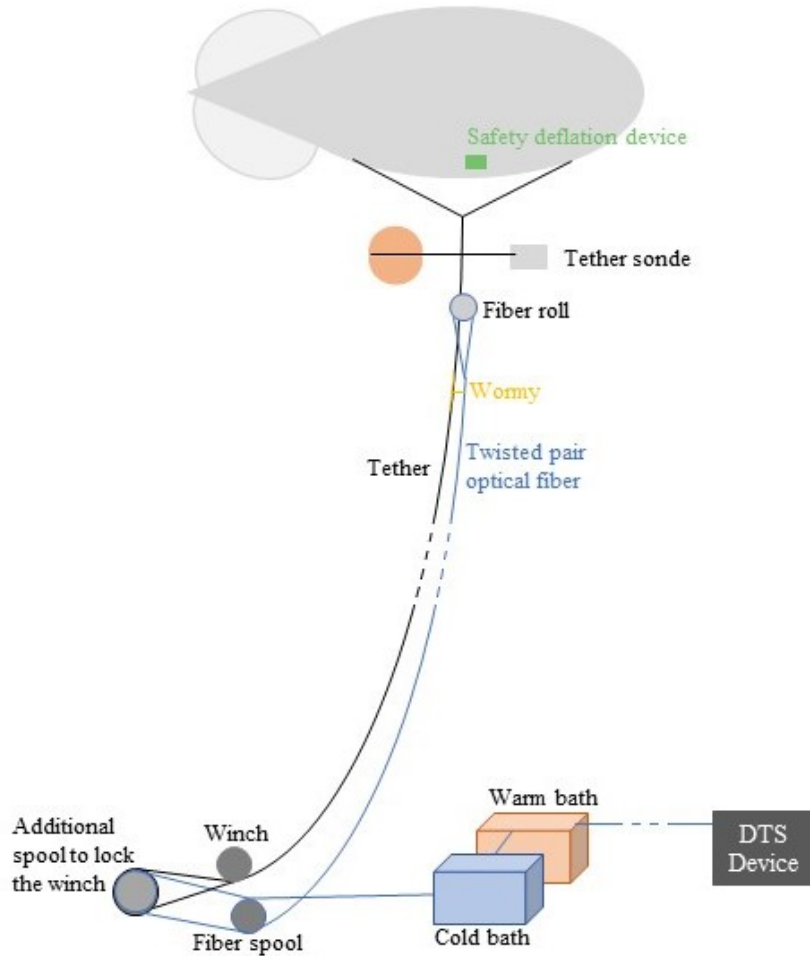


Figure 3: Sketch of the FlyFox-V set-up

With the help of a winch, a tethered balloon was launched to about 200 m. As a safety provision, a safety deflation device (see Section 4.3.1) was installed directly on the balloon and was switched on during each flight.

Shortly underneath the balloon a tether sonde was attached to the tether which functioned as a reference sensor (see Section 4.3.2). The optical fiber was placed a little further down along the tether. A twisted pair PVC fiber was used which means two separate optical fibers were twisted around each other. On top, the ends of these two fibers were spliced together around a fiber roll which was then attached to the tether.

The twisted fiber hang down next to the tether and was kept close to the tether with the help of wormies. These were small constructions which were connected to the tether about every 50 m and had a spiral where the fiber was lead through. Still, the fiber was not parallel to the tether as no tension was applied due to the move delicate nature of the used fiber.

On the ground the tether as well as the fiber were lead around an additional spool about 4 times. This procedure created enough shear to lock the balloon at a certain height and to keep the fiber in the right position.

The fiber then run through a cold and a warm water bath (see Section 4.3.3). Behind these baths, one end of the twisted pair fiber connected to the **D**istributed **T**emperature **S**ensing (DTS) device which sent out the laser pulse and measured the wavelength of its

back scatter ($P_S(x, t)$ and $P_{AS}(x, t)$ in Equation 1; see Section 4.3.4).

Figure 4 shows a picture of the actual launching area which was taken during the flight in the morning of 26th of July, 2019.



Figure 4: FlyFox-V launching area during a morning flight

When the balloon didn't fly it was fixed on the ground with two trailer nets and a rope (Figure 5). Additionally, a sand bucket of about 10 kg was always connected to it to keep it from flying away in case the net would have broken.



Figure 5: The balloon when fixed on the ground

4.3 Specification of FlyFox-V material and instruments

4.3.1 Tethered balloon and safety deflation device

The tethered balloon had a length of 6 m and a maximum radius of 2.5 m. This provided a volume of about 8 m^3 which was filled with balloon gas (90% helium) and pressurized

air. It had to be refilled about every second day to provide the needed pressure and uplift as the helium diffused out of the balloon quickly. Hence, the refilling was done with pure helium. The balloon's uplift amounted to 3 to 4 kg.

The balloon came with two outlets (see Figure 6). The first outlet (left, Figure 6) had a check valve. It was used to refill the balloon as a hose could be connected directly to it and as the air could only flow into the balloon but not out of it. The second one (right, Figure 6) consisted of a large hose which was closed with the safety deflation device (Automatic Balloon Deflation Device TTD111, Vaisala, Helsinki, Finland). This device provided the possibility of emptying the balloon extremely fast in case of an accident. To do so, the device constantly measures the pressure and opens the hose if the pressure falls below a preset threshold. For FlyFox-V this threshold was set to 900 hPa which corresponded to about 400 m above the ground.

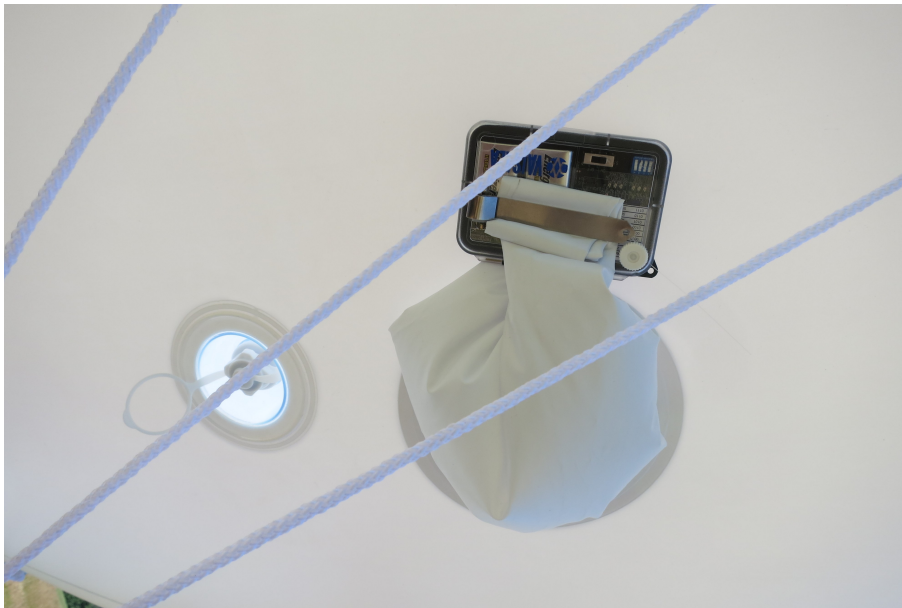


Figure 6: Outlets of the tethered balloon

4.3.2 Tether sonde

The tether sonde was mainly important for the FlyFox-V experiment as it constantly logged the pressure. By comparing this pressure to the ground pressure which was logged at the measurement tower of the LOVE project, the flying height was calculated.

The tether sonde was placed on the very top of the tether, 1.62 m from the holding lines of the balloon. Temperature, relative humidity, and air pressure were measured with an integrated reference sensor (BME280, Bosch sensortec GmbH, Reutlingen, Germany; bottomleft of Figure 7a) and wind speed was measured with a hot wire anemometer (Model Rev C, Modern Device, Providence, USA; topright of Figure 7a).

The instruments were attached to an Arduino board which logged the data at a time resolution of 1 s and sent it to a Raspberry Pi at the ground. All the electronics were surrounded by a white casing (see Figure 7b). This casing functioned as a radiation and rain shield and canalized the air flow for the sensors. To further improve the air flow towards the instruments, the tether sonde was fixed on a wind vane so it always faced in the dominating wind direction. The tether sonde held on the tether by tension but was additionally connected to it with a safety line.

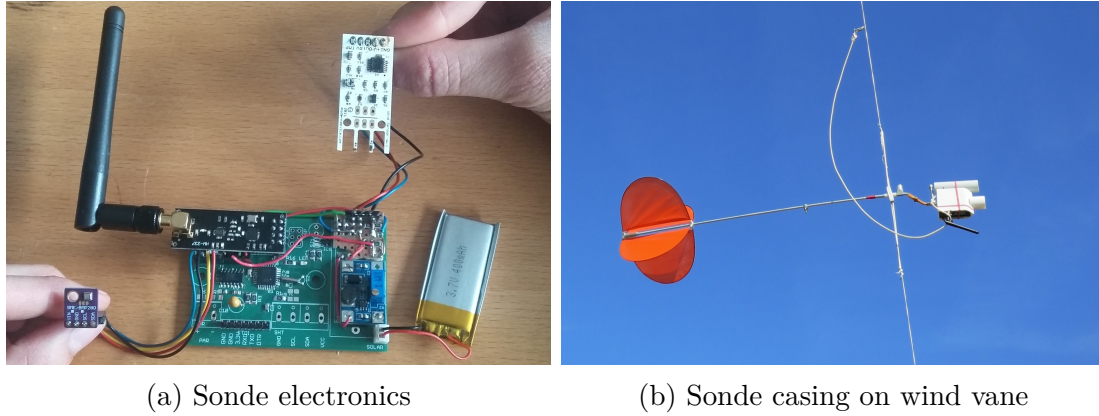


Figure 7: Tether sonde

4.3.3 Reference baths

The reference baths were needed as Equation 1 includes three unknowns (γ , $C(t)$ and the integral). Hence, three reference values at different lengths along the fiber and different temperatures needed to be known to solve it.

Two reference baths were set up from which one was heated with an aquarium heater (see Figure 8). The water in both baths was constantly moved by an aquarium pump to provide a spatially constant temperature. About 5 m of fiber were placed in eights within each bath. As the used fiber was a twisted pair fiber and actually consisted of two individual fibers, the lead through the two baths corresponded to four sections along the fiber with controlled temperatures: two at the very beginning and two at the very end of the observed interval. The temperature within each bath was measured by a thermistor (RBRsolo³, RBR Ltd., Ottawa, Canada) with a time resolution of 1s.



Figure 8: Reference baths during a flight

4.3.4 DTS device

Generally the DTS device sent out a laser pulse with an exactly known wavelength and measured the wavelength of the back scattered light. Theoretically, the back scatter of every single point along the fiber could be measured but in reality the measurement is limited by the wavelength of the used laser.

For the FlyFox-V experiment predominantly a XT-DTS (XT-DTS, Silixa, Elestree, United Kingdom) was used as a DTS device. This instrument measures at a high sampling rate and returns a temporal average every 5 seconds. For the flight on the 18th of July, 2019 a ULTIMA DTS (ULTIMA DTS, Silixa, Elstree, United Kingdom) was used which functions the same way but returns a temporal average each second.

As FlyFox-V is part of the large LOVE campaign the DTS devices never only measured the FlyFox-V but always measured other parts of the LOVE setup, too. Therefore, the XT-DTS switched between the FlyFox-V and the outer array and reported a 5-second-average every 10 seconds. The ULTIMA DTS switched between the FlyFox, the Simba south and the Rim and reported a 1-second-average every 3 seconds.

For both instruments the measurement was set up as a single-end measurement. Accordingly only one end of the fiber was connected to the DTS device and the laser was always sent in the same direction. For this type of FODS measurement it is assumed that there is no direction dependent signal loss within the optical fiber.

4.3.5 Further material

To actually launch the FlyFox-V many other items were needed which won't be specified here as they are not as important for the understanding of the experiment. A complete list of all material and its particular use is attached in the appendix (Section A).

4.4 LiDAR

As a part of the LOVE campaign, a **L**ight **D**etection **A**nd **R**anging instrument (LiDAR) was installed. It alternately observed the horizontal and vertical wind speeds between 0.025 and 5 km with a spatial resolution of 21 m. The horizontal wind speed was measured at a temporal resolution of a one minute average every 30 minutes and the vertical wind speed was measured every second.

5 Methods

5.1 Process of launching the FlyFox-V

Launching or taking down FlyFox-V required a minimum of two people and took between 45 min and 1 h. A very detailed description of all working steps is attached in Appendix B. Additionally, the documentation forms of all morning flights are attached in Appendix C.

For an experiment with a tethered balloon a permission of the "Luftfahrtamt" is required in Germany. For the FlyFox-V, this permission limited the maximum flying height to 200 m and required some safety prevention such as the safety deflation device mentioned in Section 4.2. Furthermore, it included an explicit time span when the flying was allowed. For the FlyFox-V, this time was limited by the condition of the visibility of the balloon during every flight and allowed flights from sunrise to sunset.

5.2 Processing of the DTS data

The data files written by the DTS devices included the time stamp, the LAF, the power of the stokes and anti-stokes scattering, and the temperature calculated by the instrument for each bin along the fiber.

The data from the DTS device was converted into air temperatures and combined with the data from the tether sonde, the RBRsolos³ in the reference baths and the averaged surface pressure from four barometers located near the launching area (Digiquartz Broadband Barometer Model 6000-16B, Paroscientific Inc., Redmond, USA) by Karl Lapo. For this conversion, the following steps needed to be executed for each launch:

1. Matching time stamps of all data collected during one flight
For each FlyFox launch, there was data from the DTS device, the tether sonde, the RBRsolo³ and the pressure sensors. All data sets were averaged to match the time steps of the DTS data.
2. Full matrix inversion
The full matrix inversion estimates the three unknowns of Equation 1 (γ , $C(t)$, and the integral) using three calibration baths to calculate the air temperature. All needed steps were done with the Program PyFocs by Karl Lapo and Anita Freundorf. Additionally, the measured air temperatures were converted to potential temperatures.
3. Providing every measurement with a physical location
The DTS device provides each measurement with a length an LAF to localize them. This LAF is converted to a height above ground level (see Section 5.4.2 for further details) so the data can be interpreted as temperature profiles.

5.3 Response of the balloon to the changing meteorological conditions

As a first step of the data analysis, the flying height of the balloon was investigated with a focus on its response to different meteorological parameters. The parameters which were expected to influence the balloon's movements are:

1. The horizontal wind speed at flying height
2. The vertical wind speeds around the balloon
3. The solar radiation onto the balloon

For the analysis of the balloon's response to changing horizontal wind speeds, the correlation of these wind speeds and the height offset from a maximum flying height of 200 m is observed with a scatter plot and a linear regression. To calculate the height offset (Δh), first the seven height values ($h(t)$) within the sampling period of the LiDAR are extracted. Second, the percental offset between $h(t)$ and the maximum flying height (h_{max}) of the launch is calculated ($\frac{h(t)_i - h_{max}}{h_{max}}$). Third, this percental offset is averaged and multiplied with the defined flying height of 200 m. The third step can be seen as a normalization of the height offset and is important as it excludes the influence of the overall flying height of each launch from the analysis.

$$\Delta h = \frac{\sum_{i=1}^7 \frac{h(t)_i - h_{max}}{h_{max}}}{7} * 200 \text{ m} \quad (2)$$

For the analysis of the balloon's response to changing vertical wind speeds, these wind speeds are aggregated to 10 s to match the height data. As the flying height values at this short resolution clearly aren't independent from each other, the vertical wind speeds are compared to the height change ($\delta h(t)$) since the previous measurement with help of a scatter plot. $\delta h(t)$ is calculated as:

$$\delta h(t) = h(t) - h(t - 1) \quad (3)$$

For the analysis of the balloon's response to changing solar radiation, the solar radiation directly onto the balloon would need to be known. As this isn't the case, the influence of solar radiation on the balloon's movements can not be quantified.

5.4 Method for the LAF to height conversion

The FlyFox-V data is given in the dimensions of time and LAF. Additionally, the flying height at each moment is calculated from the pressure of the tether sonde ($p_{tethered}$) and the surface pressure (p_{sfc}) by using the hypsometric equation:

$$height = \frac{(T_{mean} + 273.15) * R_a}{g_0} * \ln\left(\frac{p_{sfc}}{p_{tethered}}\right) \quad (4)$$

with T_{mean} = mean temperature of the entire profile, $R_a = 287.05 \frac{m^2}{K * s^2}$, and $g_0 = 9.81 \frac{m}{s^2}$.

To enable an analysis and interpretation of the data as temperature profiles, each measurement along the fiber needs to be matched with a height value.

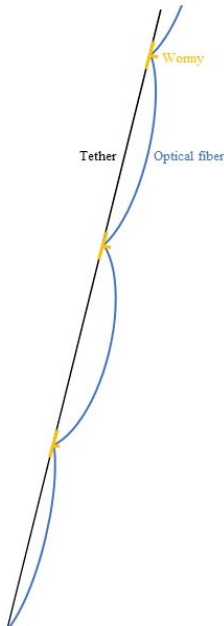


Figure 9: Schema of fiber bend

preparatory step.

During the experiment, the tether and fiber frequently looked as sketched in Figure 9. As the tether always span straight from the launching area to the balloon, its length can be determined from the maximum flying height of the launch. If the fiber optic cable had been parallel to the tether, the LAF would have corresponded to its height above ground level. However, the behavior of the fiber optic cable is harder to describe, as it was longer than the tether and bend away from its straight line between the launching area and the balloon. Furthermore, this bend of the fiber was observed to be wind speed dependent. The only locations where the fiber was strictly next to the tether were the locations of the 3 wormies, the fixation on top, and the fixation on the ground. Nevertheless, three of these locations temporally changed their position along the fiber as the fiber was only lead through the spiral of the wormies but wasn't actually fixed on it. All these observations lead to the need of an approximation to correctly convert the LAF-steps in which the data was measured into height-steps from which the data can be interpreted.

In this sections three approximations are introduced: linear, parabolic, and catenary. As they all depend upon the flying height, the uncertainty of the flying height is determined in a

5.4.1 Uncertainty of the flying height

All height approximations introduced in this section depend upon the precision of the pressure sensors at the tether sonde and the LOVE tower because the flying height used for their calculation is determined from it. For the tether sonde sensor the uncertainty is given by the manufacturer as a relative error of $\pm 0.25\%$. Hence, the standard deviation is given as

$$\sigma_{p_{tether}} = 0.0025 * \Delta p = 0.0025 * (p_{sfc} - p_{tethered}) \quad (5)$$

The uncertainty of the surface sensor is significantly lower with ± 0.02 hPa.

To quantify the uncertainty of the height, two assumptions need to be taken: First, the uncertainty of the surface pressure sensor is neglected and second, the stratification is assumed to be neutral. Therefore, the temperature gradient is assumed to be zero and the temperature (T) of the neutral layer is set to the surface temperature at the given time. The height (h) is calculated by the hypsometric equation (Equation 4). The height uncertainty (σ_{height}) results from $\sigma_{p_{tether}}$ (Equation 5) and can be calculated as:

$$\sigma_{height} = \sqrt{\left(\frac{\delta h}{\delta p_{tethered}} * \sigma_{p_{tethered}}\right)^2} = \left|\frac{(T + 273.15) * R_a}{g_0} * \frac{\sigma_{p_{tether}}}{p_{tether}}\right| \quad (6)$$

The uncertainty at the flying height propagates to the calculated height of each measurement point. This propagation of uncertainty is assumed to be linear.

5.4.2 Linear approximation

For all data, the height of each measurement was calculated by using a linear approximation. The linear approximation is the easiest approximation as it is assumed that the course of tether and fiber are identical and a straight line from the launching area to the balloon. The idea of this approximation is to create a framework of equidistant height steps and to fill it with the temperature data measured at these heights. If the balloon doesn't fly at its maximum flying height this framework includes NAs for all heights above the flying height and interpolates between the measurements to determine for its equidistant height steps. For a better understanding all calculation steps are additionally visualized in Figure 10.

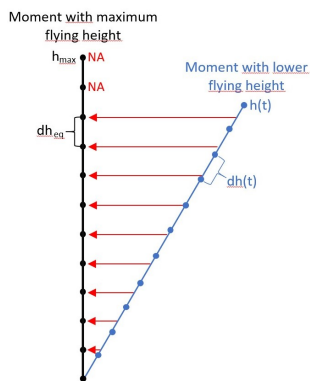


Figure 10: Schema of linear height approximation

The equidistant height steps (dh_{eq} , black Figure 10) of this framework are calculated by dividing the maximum flying height of the launch (h_{max}) by the number of LAF steps within the profile (n_{LAF}):

$$dh_{eq} = \frac{h_{max}}{n_{LAF}} \quad (7)$$

For all measurements with the balloon flying at its maximum height, this equation returns the height values of each measurement. For all moments when the balloon didn't fly at maximum flying height three more steps need to be executed: First, the calculation of the height steps between the measurements at this particular moment (blue Figure 10). Second, the interpolation of the temperature between two adjoining measurements. Third, the extraction of the

temperature data at the height of the framework (red Figure 10).

The first step is done by dividing the flying height at the given moment ($h(t)$) by the number of LAF steps within the profile:

$$dh(t) = \frac{h(t)}{n_{LAF}} \quad (8)$$

The second step is done by calculating the temperature gradient between two adjoining measurements:

$$\frac{\Delta T}{\Delta h} = \frac{T_2 - T_1}{h_2 - h_1} \quad (9)$$

The last step is done by calculating the temperature at each equidistant height step ($T(h_{eq})$) of the framework with the help of the linear interpolation:

$$T(h_{eq}) = (h_{eq} - h_1) * \frac{\Delta T}{\Delta h} + T_1 \quad (10)$$

For the comparison of the linear, parabolic and catenary height approximation, three particular moments are investigated. In these three cases, the height steps of the linear approximation are solely calculated by Equation 8.

5.4.3 Parabolic approximation

Under more windy conditions, the fiber bent away from the tether. As the tether itself wasn't vertical then but stood in angles up to 56.1° from vertical (24th of July, 18:35:00 UTC), the fiber was nearly vertical in the upper regions between two fixations but bent more strongly towards the tether in the lower regions. According to these observations, a description of the fiber course with a parabolic function was tested. This bend leads to unequal height-steps which are small close to the ground and get bigger with increasing height. As this approximation is more complicated than the linear approximation, it will only be tested for the interval between the launching area and the first wormy.

To calculate the height of the measurements with the parabolic approximation, the following four steps need to be taken: First, the parametrization of the parabolic function. Second, the calculation of the number of LAF steps within the observed height interval and their length along the parabolic function. Third, the iterative calculation of the horizontal location (x) of each measurement. Fourth, the calculation of the height of each measurement with the parabolic function defined in step one.

The parabolic approximation bases on the equation

$$z(x) = ax^2 + bx + c \quad (11)$$

The parameter a widens or closes the parabola. Parameter b moves its vertex horizontally and parameter c moves it vertically. As the lowest known point along the parabola - the location of the launching area - was set to $P_1(0|0)$ in the Cartesian coordinate system, the parameters b and c were set to 0.

Hence, only parameter a had to be adjusted by defining another known point P_2 on top of the parabola. For this point, the location of the first wormy was taken. It is known that the wormy is located at a tether length ($L_{tether}(wormy)$) of about 50 m. However, the horizontal and vertical location of the wormy varied with the angle (α) between the vertical and the tether resulting from changing meteorological conditions. Therefore, to

determine a , this angle (α) is determined first by the trigonometric relationship between the vertical line from the launching area to the maximum flying height (h_{max}) and the line from the launching area to the actual flying height ($h(t)$):

$$\alpha = \arccos\left(\frac{h(t)}{h_{max}}\right) \quad (12)$$

With α , the horizontal (x_w) and vertical (z_w) location of the wormy are calculated as:

$$x_w = L_{tether}(wormy) * \sin(\alpha) = 50 \text{ m} * \sin(\alpha) \quad (13)$$

$$z_w = L_{tether}(wormy) * \cos(\alpha) = 50 \text{ m} * \cos(\alpha) \quad (14)$$

With this, the location of the wormy is defined as $P_2(x_w|z_w)$. Knowing this second point along the parabola, the parameter a can be calculated and the function for the parabolic approximation is then defined as:

$$z(x) = \frac{z_w}{x_w^2} * x^2 \quad (15)$$

Next, the number of LAF steps within the parabola is calculated. To do so, first the length of the entire tether (h_{max}) is divided by the number of LAF steps (n_{LAF}) within the entire profile to get the linear approximated length of one LAF step. Second, the length of the tether between the launching area and the first wormy ($L_{tether}(wormy)$) is divided by this length of one LAF step to calculate the number of LAF steps ($n_{LAF}(wormy)$) within this section:

$$n_{LAF}(wormy) = \frac{L_{tether}(wormy)}{\frac{h_{max}}{n_{LAF}}} = \frac{50 \text{ m} * n_{LAF}}{h_{max}} \quad (16)$$

Nevertheless, the length of each LAF step along the parabolic function (L_{LAF}) needs to be longer than the LAF step of the linear approximation ($\frac{h_{max}}{n_{LAF}}$) as the overall length L of the parabolic function is longer than the overall length of the line. L is calculated by a line integral from $x_1 = 0$ to $x_2 = x_w$ and L_{LAF} is calculated as:

$$L_{LAF} = \frac{L}{n_{LAF}(wormy)} = \frac{\int_{x_1=0}^{x_2=x_w} \sqrt{1 + z'(x)^2} dx}{n_{LAF}(wormy)} \quad (17)$$

In the next step, the x-location at the starting point (x_1) of each LAF step is set and the end point (x_2) is calculated by iterating the line integral until:

$$\int_{x_1}^{x_2} \sqrt{1 + z'(x)^2} dx = L_{LAF} \pm 0.0005 \quad (18)$$

For the first LAF step, x_1 is set to 0 and the iteration of x_2 starts at 0.02. If Equation 18 is not fulfilled, x_2 is adjusted as

$$x_2(iteration2) = x_2(iteration1) - \frac{\int_{x_1}^{x_2(iteration1)} \sqrt{1 + z'(x)^2} dx - L_{LAF}}{6} \quad (19)$$

until it is fulfilled. The subtraction in Equation 19 is needed to make the iteration solvable and to minimize the number of iterations needed.

As soon as Equation 18 is fulfilled, the iteration of the next LAF-step-boundaries

starts with:

$$x_1(step2) = x_2(step1) \quad (20)$$

$$x_2(step2) = x_2(step1) + 0.02 \quad (21)$$

After this iteration, the x coordinate of each measurement is given and the height (z) is calculated with Equation 15.

5.4.4 Catenary approximation

The third and last height approximation works with a so called catenary function. In geometry, a catenary function describes the idealized course of a hanging chain which is only supported at its two ends. To adapt it to the FlyFox-V experiment, the fiber is assumed to be one half of a hanging chain and hence the description of the course of the fiber with a catenary function was tested. The catenary function bases on a cosinus hyperbolicus and is defined as:

$$z(x) = a * \cosh\left(\frac{x}{a}\right) + c \quad (22)$$

The parameter a widens or closes the cosinus hyperbolicus function and moves its vertex in the vertical direction. The parameter c moves the vertex in the vertical direction, too, and is introduced to enable a match of the vertex to the origin of the Cartesian coordinate system.

The known points were selected as for the parabolic approximation: $P_1(0|0)$ and $P_2(x_w|z_w)$. To place the vortex of the catenary function in the origin of the Cartesian coordinate system, the parameter c needs to equal $-a$. As there is no numeric solution to calculate parameter a , this is done by iterating Equation 22 for P_2 :

$$z_w = a * \cosh\left(\frac{x_w}{a}\right) - a \quad (23)$$

The height for each measurement along this function is calculated with the same steps as done for the parabolic approximation (Equation 16 to 21).

5.4.5 Comparison of approximations

After the three different height approximations are fitted, they are compared to each other for three different measurements. The conditions of these measurements varied by the intensity of the horizontal wind speed and hence by the angle α between the vertical and the tether. The course of the tether, the temperature profile, and the vertical distance between the non linear and the linear height approximation is investigated to decide on the best non linear approximation and on a threshold between the linear and the non linear approximation.

5.5 Investigation of the stable boundary layer

From the FlyFox data, the static stability of the lower atmospheric boundary layer is analyzed as the static stability can be used to identify the SBL and the MBL. The static stability can be determined from the change of potential temperature with height ($\frac{\delta\theta}{\delta z}$). In this case, the height is calculated by the linear approximation introduced in Section 5.4.2.

By definition, $\frac{\delta\theta}{\delta z}$ is positive for statically stable stratified air layers. The positive gradients imply that an air mass which gets lifted from its original position will be cooler than its new surrounding. It therefore has a higher density than the surrounding air and will fall back to its former height position. Hence, small movements don't have a great influence on the air layer and the stratification in it is called stable. The threshold for defining a stratification as stable is given by

$$\frac{\delta\theta}{\delta z} \geq 0.01 \frac{K}{m} \quad (24)$$

The large stable stratified air layer that builds up near the surface during the night is called the stable boundary layer (SBL). The SBL doesn't have to solely include stable stratified air layers but can also include smaller regions with neutrally stratified air where

$$-0.01 \frac{K}{m} < \frac{\delta\theta}{\delta z} < 0.01 \frac{K}{m} \quad (25)$$

or even slightly unstable regions where

$$\frac{\delta\theta}{\delta z} \leq -0.01 \frac{K}{m} \quad (26)$$

Nevertheless, the dominating regime needs to be the stable stratification. As soon as the stratification is dominated by neutral or unstable conditions, the end of the SBL is reached.

As a preparation for the further analysis, $\frac{\delta\theta}{\delta z}$ is calculated. As the instrument noise highly influences finite temperature differences between adjoining measurements, the potential temperature is averaged over 4 m by a moving window approach before $\frac{\delta\theta}{\delta z}$ is calculated.

5.5.1 Influence of height approximations

As the main focus while observing the stability of the ABL relies on $\frac{\delta\theta}{\delta z}$, the uncertainty in estimating the height (z) of each measurement needs to be considered. Due to this, the influence of the height approximations on the gradients in potential temperatures is explored.

The same three measurements are used as for the observation of the LAF to height conversion in Section 5.4. For each measurement, $\frac{\delta\theta}{\delta z}$ is calculated twice: first with the linear approximated height and second with the height calculated by the approximation chosen as the best one for the given conditions. Furthermore, the difference between the two gradients is calculated as

$$\Delta \frac{\delta\theta}{\delta z} = \frac{\delta\theta}{\delta z}(\text{linear}) - \frac{\delta\theta}{\delta z}(\text{nonlinear}) \quad (27)$$

For the observation of the SBL, the classification as stable, neutral, or unstable is more important though than the actual value of $\frac{\delta\theta}{\delta z}$. Therefore, it is analyzed how often using the linear approximation classifies measurements as stable while using the non linear approximation does not or vice versa as this could influence the determination of the SBL extent.

5.5.2 The morning transition

The first scientific research question asks whether the **M**orning **T**ransition (*MT*) observed by the traditional surface observations matches the MT observed by FlyFox. To answer this question, the time of the MT is determined from the sensible heat flux (H) near the surface. The needed data was collected by a CSAT (CSAT3, Campbell scientific, Bremen, Germany) installed at the tower of the LOVE project in 1.25 m height above the ground. The moment when H changes its direction is defined as the MT [3].

There were three expectations as listed in Section 2: the first one on the direction change of H is answered while determining the MT. The second one on the time lag between sunrise and MT is investigated by determining this time lag for the observed mornings. The third one on the wind speed dependency of the MT is tested by a comparison of the MT to the horizontal wind speed data collected by the CSAT in 1.25 m height.

The MT is then compared to the observations gained from FlyFox-V. The MT aims to define the bottom start of the transformation of the nocturnal SBL characterized by a stable stratification into the daytime MBL characterized by a neutral or unstable stratification. Hence, the spatially-distributed evolution of $\frac{\delta\theta}{\delta z}$ is observed to validate this change in the stability regime.

As will be seen later, the definition of the MT as a moment in time is not the best fitting definition to describe the observed process. The MT can rather be defined as a **M**orning **T**ransition **P**hase (MTP) of a defined temporal and spatial scale [1]. Hence, these scales on which the SBL turns into a MBL in the morning are investigated: The overall temporal and spatial scale of the MTP is visually estimated from $\frac{\delta\theta}{\delta z}$ for all morning flights. The start of the MTP is defined as the moment when the magnitude of the nocturnal SBL decreases. The end of the MTP is defined as the moment when no clear temporally and spatially connected stable layer can be identified. In addition to the determination of the scales of the MTP, a transition velocity is calculated to indicate how fast the thickness h of the SBL decreases:

$$v = \frac{\Delta h(SBL)}{\Delta t} \quad (28)$$

From $\frac{\delta\theta}{\delta z}$ will be seen that the transformation from a SBL to a MBL occurs simultaneously at the upper and the lower boundary of the SBL. Therefore, the changing velocity of each boundary height is calculated to enable a comparison of the importance of both processes.

5.5.3 Bottom-up approach

The second scientific research question asks whether the occurrence and movement of distinct air layers is induced by surface processes. To investigate this bottom-up approach, three internal layers of the SBL of the 22nd of July are selected (Section 6.5.4, Figure 30). These layers are clearly distinguishable from each other by their static stability: Layer 1 is strongly stable with $\frac{\delta\theta}{\delta z} > 0.1\frac{K}{m}$, Layer 2 is less stable or even neutral with $0.1\frac{K}{m} > \frac{\delta\theta}{\delta z} > -0.01\frac{K}{m}$, and Layer 3 is strongly stable again with $\frac{\delta\theta}{\delta z} > 0.1\frac{K}{m}$.

For the time these three layers appear, the data collected by four CSATs in 0.5, 1.25, 4 and 12 m height is investigated. The variables wind speed (mean horizontal, mean vertical, and standard deviation vertical), sonic temperature, buoyancy flux and momentum flux are visually investigated for a relationship to the occurrence of the different layers. Additionally, the wind direction is investigated to decide whether the occurrence of the

three layers can rather be explained by advection than by purely vertical transport or generation.

6 Results and Interpretation

6.1 Evaluation of the experimental set-up

The FlyFox-V experiment gives great insights in the temperature profile of the lowest 200 m of the ABL. Nevertheless, some improvements can be implemented for further deployment.

First, it was very uncertain to only measure the launching height of the balloon by the pressure data of the tether sonde and to define the locations of the wormies by it. It would be better if a mark was placed every 50 m along the tether to ensure that the wormies are always at the same height which additionally is precisely known. Furthermore, this approach would simplify the launching of the balloon to a maximum height of 200 m as the influence of the wind speed on the flying height can be excluded. With only using pressure as a height measurement, the balloon was fixed at a height of 200 m a.g.l. under the meteorological conditions during the launch and not at 200 m maximum flying height under windless conditions. Additionally, no receiver for the tether sonde and no laptop would be needed at the launching area if the height was defined by the marks. Hence, a mark should be set at the location of each wormy and one at 200 m or the chosen maximum flying height, respectively.

Second, the wind sensor of the tether sonde was not calibrated during the FlyFox-V experiment. Therefore, the information on the wind speeds at flying height was received but couldn't be interpreted. This should be done in advance for the next experiment to simplify and to specify the correlation of the horizontal wind speed and the flying height of the balloon.

Third and most important, only one fiber should be used for the next FlyFox experiment which does not have a splice at the top of the profile. For FlyFox-V a twisted pair fiber was used. This fiber consisted of two separate fibers which were wrapped around each other and got spliced together at the top of the profile. These two fibers were of the exactly same type but nevertheless showed a different differential attenuation. The reference baths were positioned in a way that each optical fiber only passed through each bath once. Resulting from this, the differential attenuation of each fiber could not precisely be quantified as three known sections would be needed for it. To improve upon this, the optical fiber of the next FlyFox experiment should not be spliced on top of the profile to ensure that two reference sections are provided near the start and end of the fiber.

6.2 Response of the balloon to changing conditions

This section deals with answering the first methodological research question on how the balloon responds to changing vertical and horizontal wind speeds. As stated in Section 5.3, the wind speeds are measured by the LiDAR and the height is determined from the pressure sensors. The expectation was that the horizontal wind speed would influence the movement of the balloon more than the vertical wind speed.

For the investigation of the influence of the horizontal wind speed, the height offset to a maximum flying height of 200 m is calculated from the data of the 18th, 22nd, and 26th of July (see Section 5.3) and plotted against the horizontal wind speed. A linear model is

fitted under the condition of the height offset (Δh) being proportional to the horizontal wind speed (u) and is added to the scatter plot (Figure 11). This linear regression predicts a relationship of

$$\Delta h = -3.025 * u + 0.708 \quad (29)$$

The intercept in this case isn't significant. Additionally, it does not make any physical sense as it predicts a positive offset from the maximum flying height of 0.708 m at $0 \frac{m}{s}$ wind speed which is not possible. Nevertheless, the slope of the linear model has a p-value of $1.026 * 10^{-7}$ which makes it highly significant. Due to this, the influence of the horizontal wind on the flying height of the balloon must be considered. An increase of the horizontal wind speed of $1 \frac{m}{s}$ corresponds to a lowering of the balloon by around 3 m at a flight with 200 m maximum height.

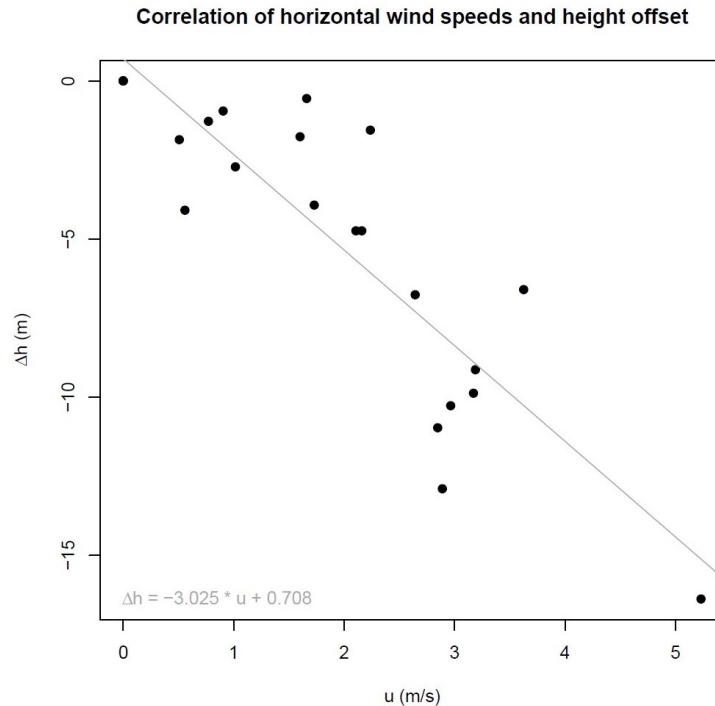


Figure 11: Correlation of horizontal wind speed and height offset from 200 m

For the investigation of the influence of the vertical wind speed, only the data from the 22nd of July is used. The height difference between one height measurement and its previous measurement (δh) is determined and plotted against the vertical wind speeds (w , Figure 12). In contrast to Figure 11, the scatter plot of w against δh does not show any correlation between the two quantities and hence no linear regression is fitted.

In summary, it can be stated that in Voitsumra only the horizontal wind speeds need to be considered for determining the flying height and the movement of the tethered balloon. This result is not surprising as the vertical wind speeds only range from $-0.058 \frac{m}{s}$ to $0.147 \frac{m}{s}$ while the horizontal ones range from $0 \frac{m}{s}$ to $5.231 \frac{m}{s}$. This finding can only be transferred to other balloon experiments if the experimental site there shows a similar ratio of horizontal to vertical winds. If stronger vertical winds appear this factor may not be negligible.

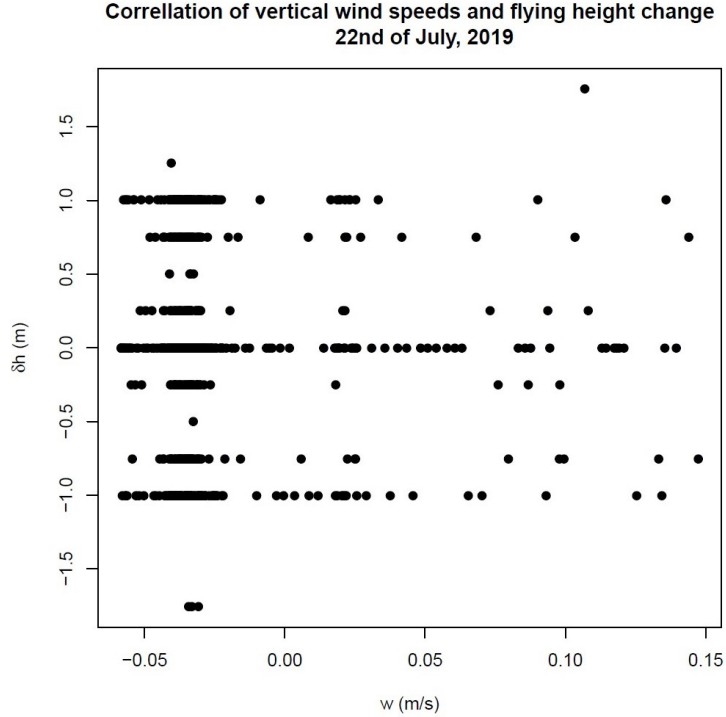


Figure 12: Correlation of vertical wind speed and height change since the previous measurement

6.3 LAF to height conversion

This section deals with the second methodological research question of the LAF to height conversion. The three height approximations introduced in Section 5.4 are fitted and compared. For this analysis, the data of the ascending profile of the launch on the 22nd of July is used. The most important parameter that influences the choice of the best approximation is the horizontal wind speed and hence the angle (α) between the tether and the vertical. Therefore, three measurement times were taken with the angle being 10 °(03:45:30 UTC), 15 °(03:34:10 UTC) and 22.6 °(03:18:40 UTC), the last being the largest angle that appeared that day. The comparison covers for the lowest section of the fiber between the launching area and the first wormy. It is assumed that the wormy was fixed at a tether length of exactly 50 m.

6.3.1 Calculated parameters of the approximations

All parameters calculated for the three approximation at the three measurement times are listed in Table 1.

6.3.2 Comparison of approximations

To compare the three approximations, one figure was created for each observed angle between the tether and the vertical. Within this figure, three plots are combined:

1. Course of the fiber

The left plot shows how the fiber bends away from the tether. The location of the launching area and the location of the first wormy are marked with black dots.

| time (UTC) | 03:45:30 | 03:34:10 | 03:18:40 |
|---------------------------------------|-----------------|-----------------|-----------------|
| α | 10 ° | 15 ° | 22.6 ° |
| Linear height approximation | | | |
| $h(t)$ | 179.53 m | 176.09 m | 168.26 m |
| n_{LAF} | 728 | | |
| L_{LAF} | 0.2466 m | 0.2419 m | 0.2311 m |
| Parabolic height approximation | | | |
| x_w | 8.55 m | 12.50 m | 17.76 m |
| z_w | 49.24 m | 48.30 m | 46.15 m |
| $n_{LAF}(wormy)$ | 200 | | |
| $z(x)$ | $0.674 * x^2$ | $0.309 * x^2$ | $0.146 * x^2$ |
| L | 50.59 m | 50.92 m | 51.01 m |
| L_{LAF} | 0.2534 m | 0.2551 m | 0.2555 m |
| Catenary height approximation | | | |
| a | 2.2320361712 | 3.7674300000 | 6.3342103886 |
| L | 51.42 m | 51.93 m | 52.10 m |
| L_{LAF} | 0.2575 m | 0.2601 m | 0.2609 m |

Table 1: Parameters of the linear, parabolic and catenary height approximation

2. Temperature profile

The middle plot shows the temperature of each measuring point plotted against the height calculated with the respective approximation. The temperature profile is the profile measured at the time when the observed angle appeared and varies for the three figures.

3. Difference to linear approximated height and standard deviation

The right plot shows the vertical offset between the linear approximated height and the non linear approximated height for each measuring point. Additionally, the uncertainty of the height is plotted (dashed grey line) as it is a vertical offset to the linear approximated height, too. At the location of the wormy, it amounts for 12.3 cm at $\alpha = 10^\circ$, 12.1 cm at $\alpha = 15^\circ$, and 11.5 cm at $\alpha = 22.6^\circ$. To not misinterpret the plot, it must be considered that the height uncertainty does not influence the difference between the linear and the non-linear approximated heights as it influences both values the exactly same way.

In addition, a specific measurement point is highlighted in all plots in order to simplify the linking of the information between the plots. The highlighted measurement points are placed on interesting and well visible features in the temperature profile and vary for the three figures.

LAF to height conversion for $\alpha = 10^\circ$

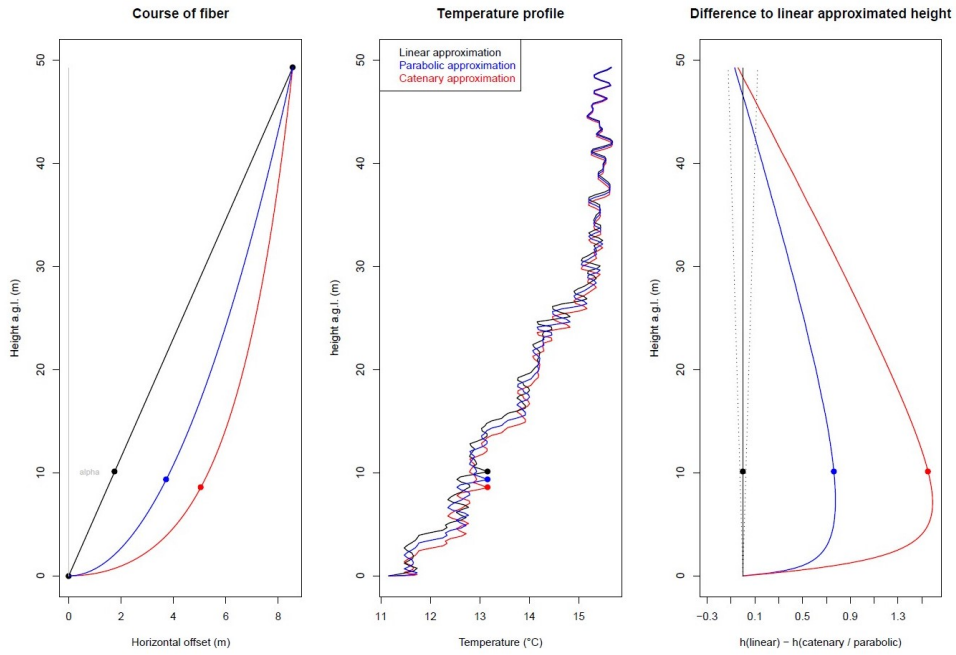


Figure 13: Comparison of the three height approximations for $\alpha = 10^\circ$

LAF to height conversion for $\alpha = 15^\circ$

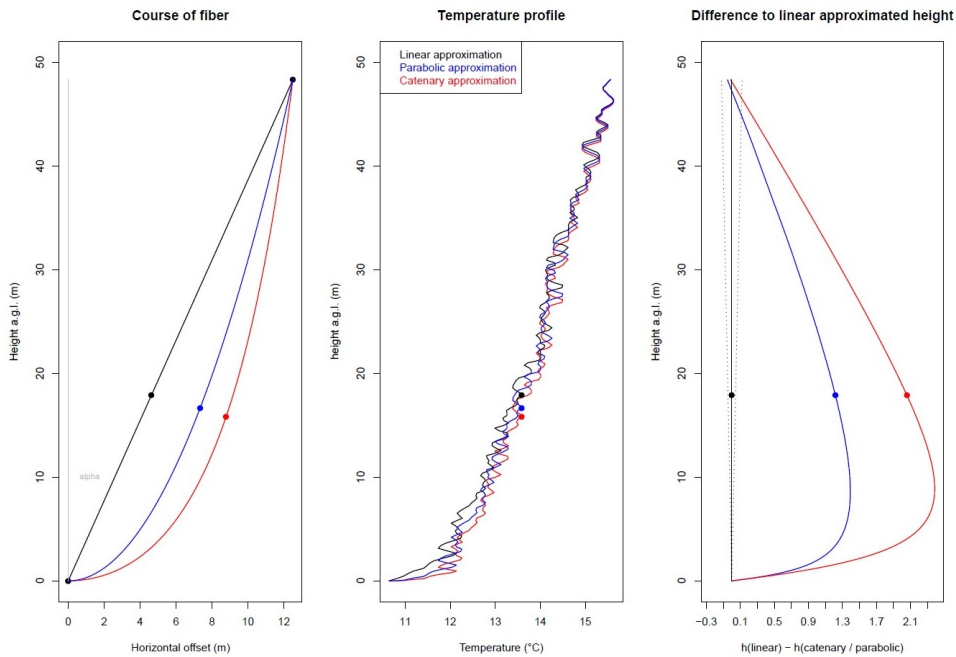
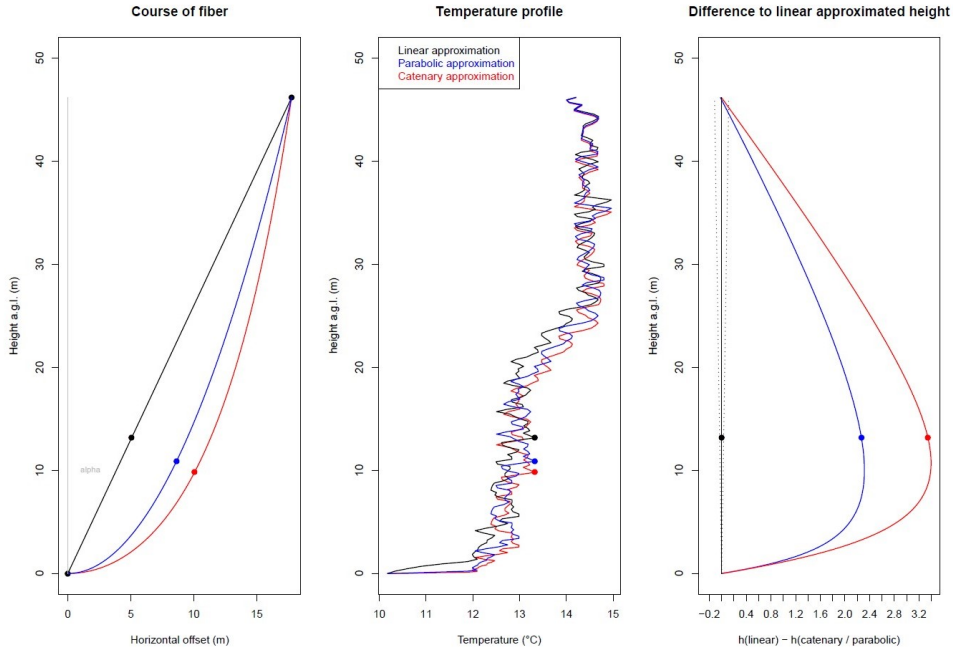


Figure 14: Comparison of the three height approximations for $\alpha = 15^\circ$

Figures 13 to 15 show that the linear and the two non-linear approximations lead to three different temperature profiles. For all wind regimes, these profiles vary most in the regions close to the surface and get more similar in the higher regions which results from the shape of the non-linear functions. The greatest height difference between the linear approximated height and the non-linear approximated height (Table 2) appears within

LAF to height conversion for alpha = 22.6°

Figure 15: Comparison of the three height approximations for $\alpha = 22.6^\circ$

| | | | |
|---------------------------|----------|----------|----------|
| time (UTC) | 03:45:30 | 03:34:10 | 03:18:40 |
| α | 10 | 15 | 22.6 |
| maximum height difference | | | |
| parabolic | 0.775 m | 1.393 m | 2.315 m |
| catenary | 1.590 m | 2.385 m | 3.396 m |

Table 2: Maximum offset between the linear and the non-linear approximated heights

the lowest 5 to 15 m for both approximations and all three wind regimes. It increases with increasing wind speeds or angles, respectively.

The small height difference at the very top of the profile results from the method used to determine the non-linear heights. The heights were calculated by iteration with an accepted uncertainty of ± 0.0005 m for each LAF step which amounts for ± 0.1 m after the 200 LAF steps within the observed tether section. Hence, the calculated height offset at the location of the wormy can be neglected.

6.3.3 Interpretation of the LAF to height conversion

From the observations during the experiment, it follows that two different approximations for the LAF to height conversion are needed: one for situations with weak wind and one for situations with strong winds. For weak winds, the linear approximation is chosen to be the best approximation: During the experiment, it has been observed that the balloon flew nearly vertically above the launching area and the fiber hang down close to the tether when nearly no winds occurred. Hence, the fiber can be assumed to be identical to the line between the launching area and the balloon and the height of the measurements along the fiber can be approximated linearly. For strong wind speeds, the balloon didn't fly vertically above the launching area and the fiber bend away from the tether. This lead

to the need of a non-linear approximation and a threshold between the weak and strong wind conditions.

The decision on the best non-linear approximation is mainly influenced by two criteria: First, the length of the modeled fiber needs to meet the actual length of the fiber used in the experiment. Second, the horizontal offset between the linear approximation which represents the tether and the non-linear approximation which represents the fiber mustn't be too large as this wasn't observed in the field.

To ensure the correct fiber length, each LAF step would need to equal 0.254 m as this is the known physical distance between two measurements. For all situations the parabolic approximation meets this condition best as it calculates LAF steps between 0.2534 and 0.2555 m. The linear approximation models too short LAF steps between 0.2466 and 0.2340 while the catenary approximation models too large LAF steps between 0.2575 and 0.2609 m. This indicates that the parabolic approximation works better than the catenary approximation. The choice of the parabolic approximation is confirmed by the fact that the fiber modeled with the parabolic function bends less away from the tether than the fiber modeled with the Catenary function, meeting the second criteria.

To decide on a threshold when to change from the linear to the parabolic height approximation, the vertical offset between the linear approximated height and the parabolic approximated height needs to be considered. The linear approximation is the easiest approximation and therefore has a stronger appeal. The non-linear approximation should only be used for situations when the height error which would occur under a linear approximation exceeds a threshold of ± 0.5 m. This threshold is chosen as it equals the maximum height uncertainty at a flight of 200 m height which results from the uncertainty of the pressure sensor below the balloon.

This threshold of ± 0.5 m leads to a maximum offset between the linear approximated height and the non-linear approximated height of 1 m. If the vertical offset exceeds 1 m at any height, the linear approximation should not be used but the parabolic one. In the observed situations, the greatest vertical offset between the linear approximated height and the parabolic approximated height amounts for 0.775 m at $\alpha = 10^\circ$, 1.394 m at $\alpha = 15^\circ$, and 2.315 m at $\alpha = 22.6^\circ$. This leads to the conclusion that the linear approximation is valid for situations with angles up to 10° and that the parabolic approximation needs to be used for situations with angles greater than 10° . For a flight at 200 m, a 10° angle corresponds to a lowering of the balloon by about 3 m. According to Section 6.2, this lowering corresponds to a horizontal wind speed of about $1 \frac{m}{s}$.

From the data, it can be assumed that also slightly windier conditions could be approximated linearly as the threshold of a maximum height difference of 1 m has not been exceeded at $\alpha = 10^\circ$. To decide on this more precise threshold, more angles between 10° and 15° would need to be modeled and their maximum height offset would need to be calculated. From the given data though, 10° is the best threshold to choose as the height offset is closer to 1 m and hence less situations get excluded from the linear approximation than would get included for it if 15° was chosen as a threshold. Furthermore, it is better to exclude situations from the linear approximation as the parabolic approximations is the more precise approximation with a LAF length closer to 0.254 m and an horizontal offset between fiber and tether which is closer to the offset observed during the experiment.

6.4 Temperature profiles of the lower ABL

After the LAF has been converted to a height above the ground, the FlyFox data can be interpreted as a temperature profile. For the analysis, potential temperatures (θ) are used instead of the measured air temperatures to eliminate the influence of altitude on each measurement. Figures 16 to 19 show the profiles of potential temperature during the morning flights on the 18th, 22nd, 23rd, and 26th of July. The temperature scale varies between the four plots to improve the visibility of the internal structures. Nevertheless, each color scale covers a temperature range of 17 °C to maximize the comparability of the patterns.

The coldest temperatures occurred on the 18th while the warmest temperatures occurred on the 26th of July. During all mornings the coldest temperatures were measured early in the morning and near the surface. Furthermore, all early mornings show an inversion as the cold air near the surface is covered by warmer air masses. Closer to the end of the measurement all profiles become more isotherm and the inversion disappears. This transformation from a cold air mass near the surface with an inversion layer above it to a nearly isotherm air mass is part of the morning transition which will further be investigated in Section 6.5.2.

In addition to the temporal evolution of the temperature profile, the FlyFox technique reveals internal layers of a similar temperature which can clearly be distinguished from other layers. These internal layers also show a vertical movement as e.g. well visible in Figure 18 (03:00 to 04:30 UTC, 0 to 70 m).

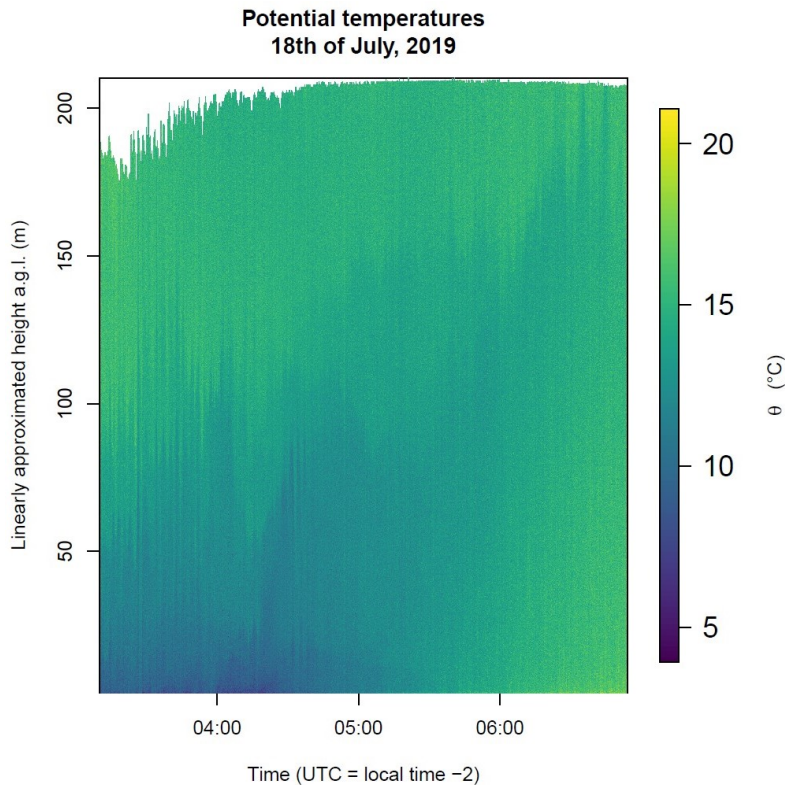


Figure 16: Profile of potential temperature on the 18th of July

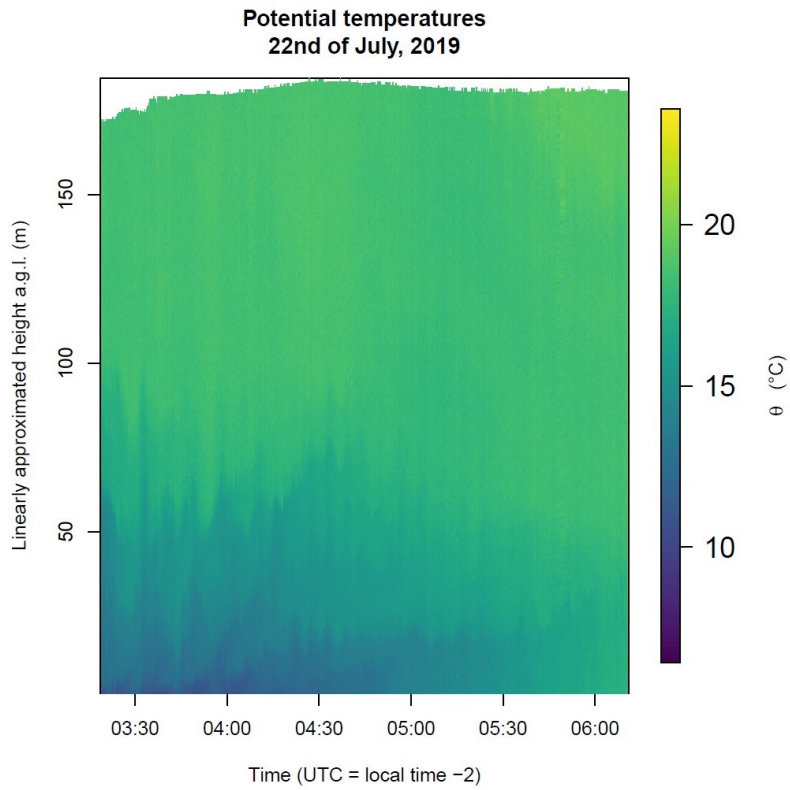


Figure 17: Profile of potential temperature on the 22nd of July

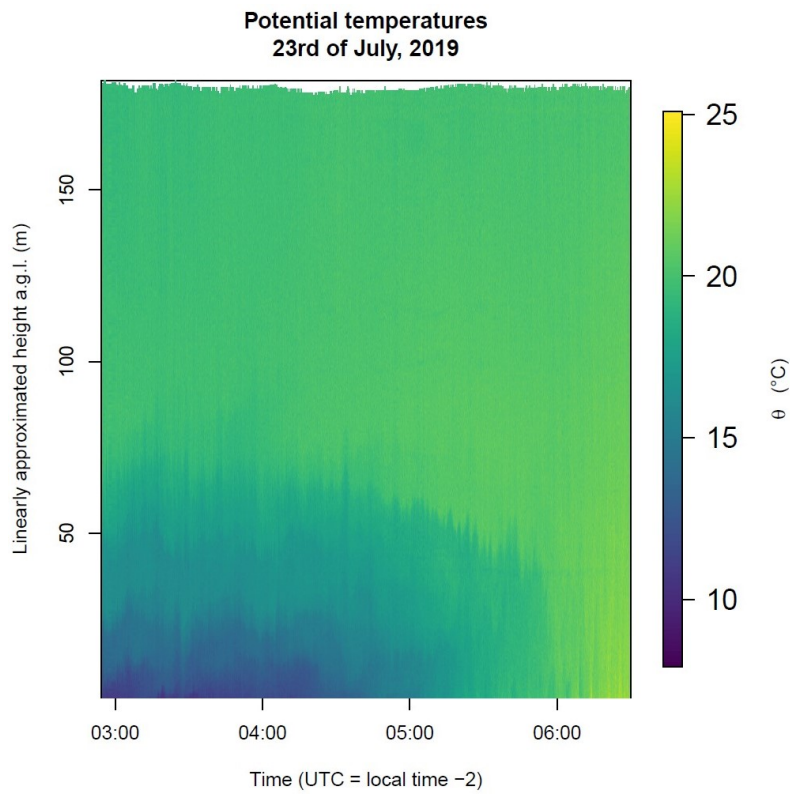


Figure 18: Profile of potential temperature on the 23rd of July

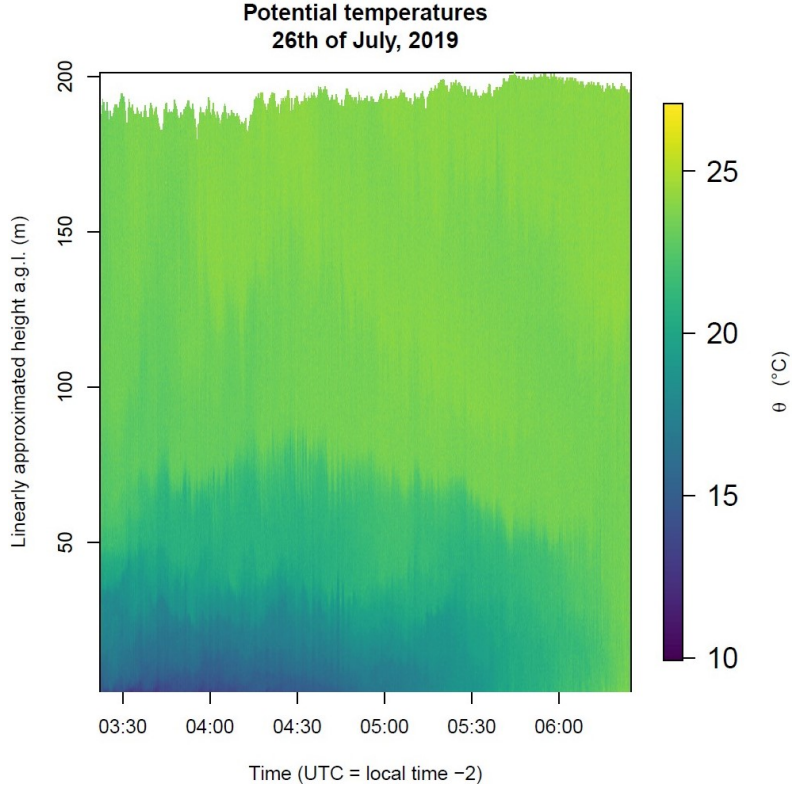


Figure 19: Profile of potential temperature on the 26th of July

6.5 Investigation of the stable boundary layer

6.5.1 Influence of height approximation

The SBL can be observed best from the gradients of potential temperatures with height ($\frac{\delta\theta}{\delta z}$). To investigate the influence of the height approximations on these gradients, a case study is conducted for the same measurement times on the 22nd of July as in Section 6.3. From these three measurements, the one with the weakest wind speeds (03:45:30 UTC, $\alpha = 10^\circ$) was excluded as the linear approximation is chosen to be the best approximation for these conditions. For the other two measurements (03:34:10 UTC, $\alpha = 15^\circ$ and 03:18:40 UTC, $\alpha = 22.6^\circ$), the parabolic approximation is decided to be the best approximation. Hence, the gradients calculated from the linear approximated height and the gradients calculated from the parabolic approximated height are compared. The difference between the two gradients is visualized in Figure 20. For both scenarios, the difference is largest close to the surface as the parabolic approximation presumes much smaller height steps there than the linear approximation. For the less windy condition, the differences of the gradients are generally smaller than for the more windy condition as the two height approximations simulate more similar scenarios. In the higher regions, the difference between the two gradients oscillates around 0 for both analyzed wind regimes. This region starts at a height of 24.5 m for the less windy situation and at a height of 34.5 m for the windier situation.

Additionally to the difference between the gradients, the classification of the air layer as stable stratified ($\frac{\delta\theta}{\delta z} \geq 0.1 \frac{K}{m}$) or neutral/unstable ($\frac{\delta\theta}{\delta z} \leq 0.1 \frac{K}{m}$) is analyzed. The gradients are plotted in Figure 21 and the threshold for the stable stratification is added to visualize when the different height approximation influences the classification of the stratification. In none of the cases, the classification of a gradient changes. Hence, the linear height

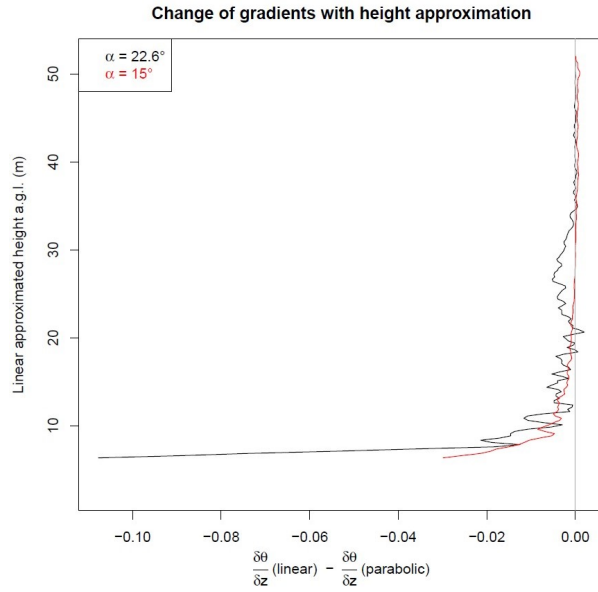
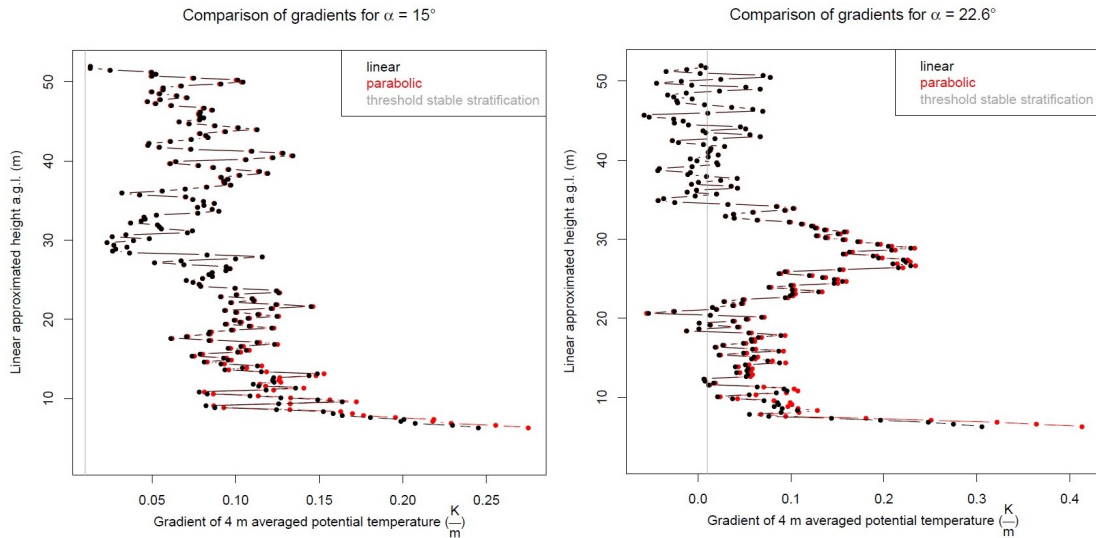


Figure 20: Difference between gradients calculated with the linear and the parabolic height approximation

approximation is considered to be precise enough to be used for answering the following research questions.



(a) Less windy condition with $\alpha = 15^\circ$ (b) More windy condition with $\alpha = 22.6^\circ$

Figure 21: Smoothed gradients of potential temperatures with linearly and parabolic approximated heights

6.5.2 The morning transition

For the four given morning flights the time of the **M**orning **T**ransition (MT) was calculated. For all days, the first expectation which stated that H would change from negative (= directed downwards) to positive (= directed upwards) at the MT could be validated.

The second expectation stated that the MT would occur more than 2 hours after sunrise. The expectation resulted from the research done by Angevine et al. (2001) and Lapworth (2006). They observed the MT in flat terrains and found mean delays between sunrise and MT of 1.3 h [1] and 2.0 h [3]. The expectation of a later MT than observed by these researchers resulted from the different topography of the experimental site. In contrast to the flat experimental sites of Angevine et al. (2001) and Lapworth (2006), a time delay was expected between the sunrise and the time when the sun actually reached the launching area due to the shading of the surrounding mountains. On the days observed by FlyFox-V, the sun rose at 03:23, 03:28, 03:29, and 03:33 UTC (dotted lines, Figure 22) while the MTs occurred at 4:32, 4:42, 4:28, and 5:00 UTC (dashed lines, Figure 22). The time span between sunrise and MT amounts for 1:09, 1:14, 1:01, and 1:27 h. Hence, the expectation could not be validated as the MT occurred earlier than expected and even earlier than predicted by the cited studies. This earlier occurrence of the MT may be "the result of differential heating in the valley, which extracts the cold air and leads to mixed-layer advection" [2].

The third expectation related to the MT stated that the MT would occur later on days with stronger winds than on days with weaker wind [3]. To verify this expectation, the 10 min averages of the horizontal wind speed measured with the CSAT in 1.25 m height are investigated (Figure 23). These measurements show that the horizontal wind

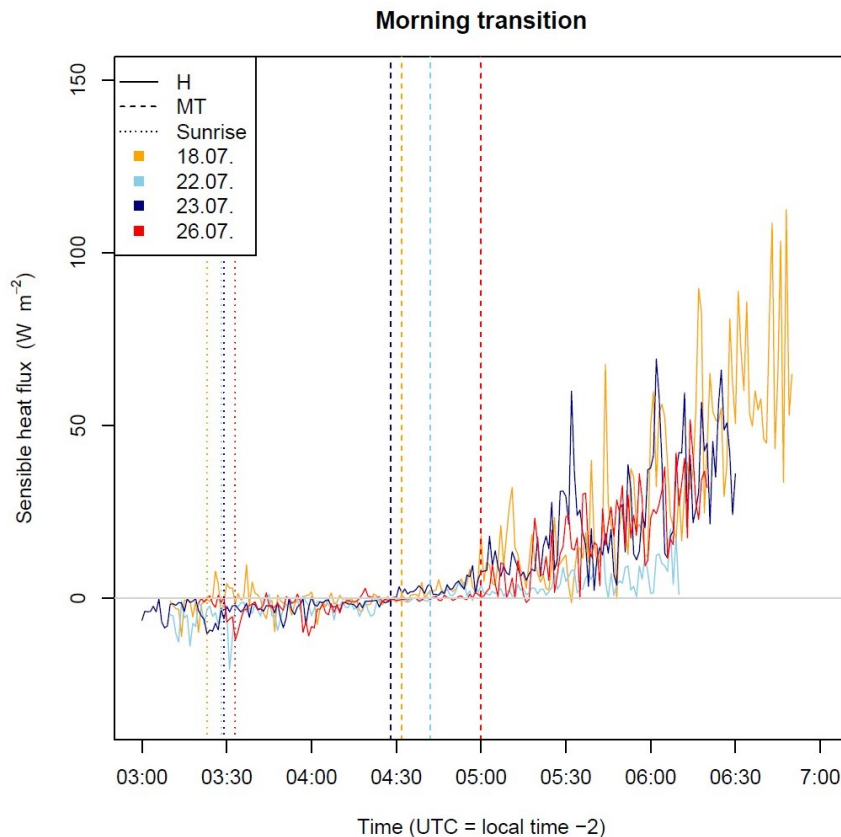


Figure 22: Sensible heat flux (solid line), MT (dashed line), and sunrise (dotted line)

speeds before the MT are the weakest for the 18th. This day has an early MT. The 22nd, 23rd and 26th show higher but at the same time very similar wind speeds. Nevertheless, their MTs differ by more than half an hour. Therefore, no clear correlation can be found between the horizontal wind speed and the time of the MT and the third expectation can not be validated.

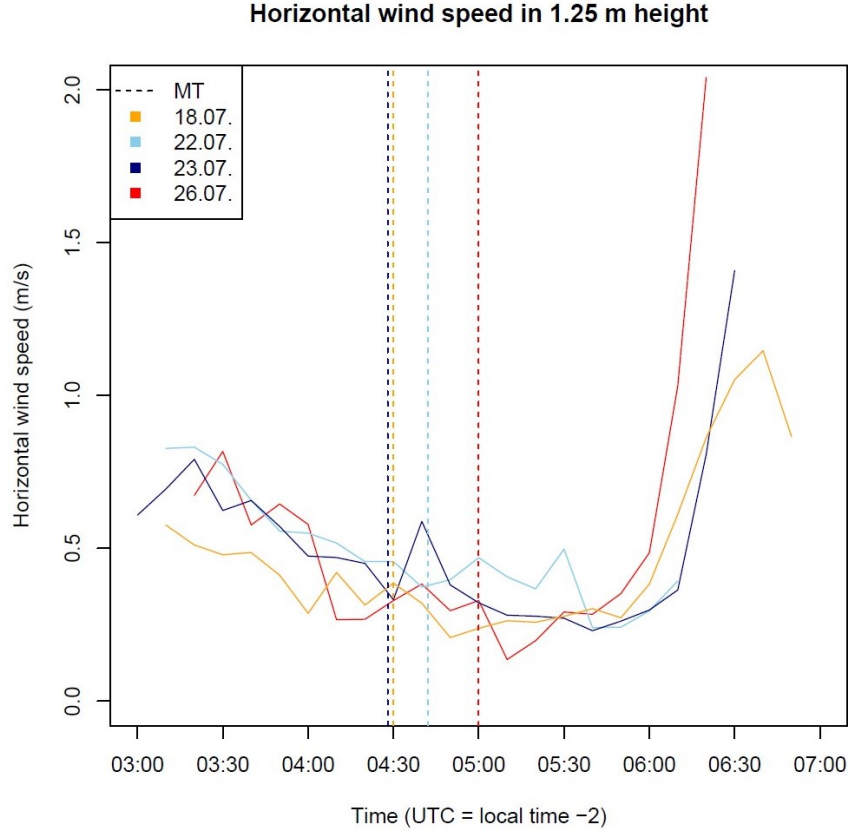


Figure 23: Horizontal wind speeds measured by the CSAT in 1.25 m a.g.l. (solid line) and MT (dashed line)

For the three results presented above it needs to be noted that very few mornings have been analyzed. This results from the number of flights done with FlyFox as the values were calculated to connect it to the FlyFox measurements. For a deeper analysis of the time of the MT in the mountain valley around Voitsumra, more mornings would need to be used for the determination of the MT.

In the next step, the time of the MT was set into the context of the $\frac{\delta\theta}{\delta z}$ -profiles observed with FlyFox (Figure 24 to 27). The solid lines in Figure 25 to 27 show an approximation

| Day of launch | Morning transition | Stability change | Time span between |
|--------------------------|--------------------|------------------|-------------------|
| 18 th of July | 04:32 UTC | 05:33 UTC | 01:12 h |
| 22 nd of July | 04:42 UTC | 04:51 UTC | 00:09 h |
| 23 rd of July | 04:28 UTC | 05:08 UTC | 00:40 h |
| 26 th of July | 05:00 UTC | 05:18 UTC | 00:18 h |

Table 3: Comparison of morning transition (1.25 m a.g.l.) and gradient change (6 m a.g.l.)

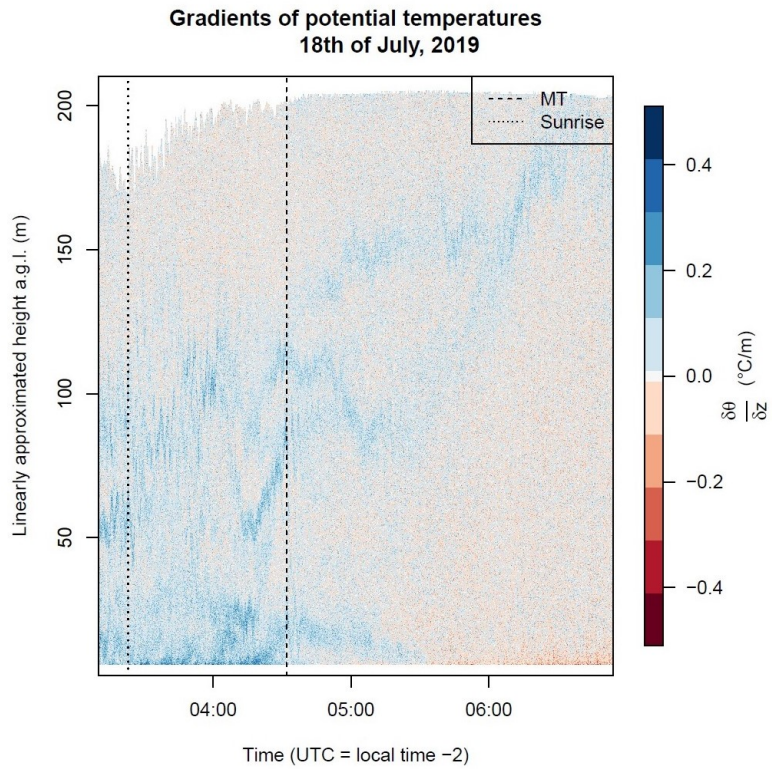


Figure 24: $\frac{\delta\theta}{\delta z}$ -profile of the 18th of July, sunrise (dotted line) and MT (dashed line)

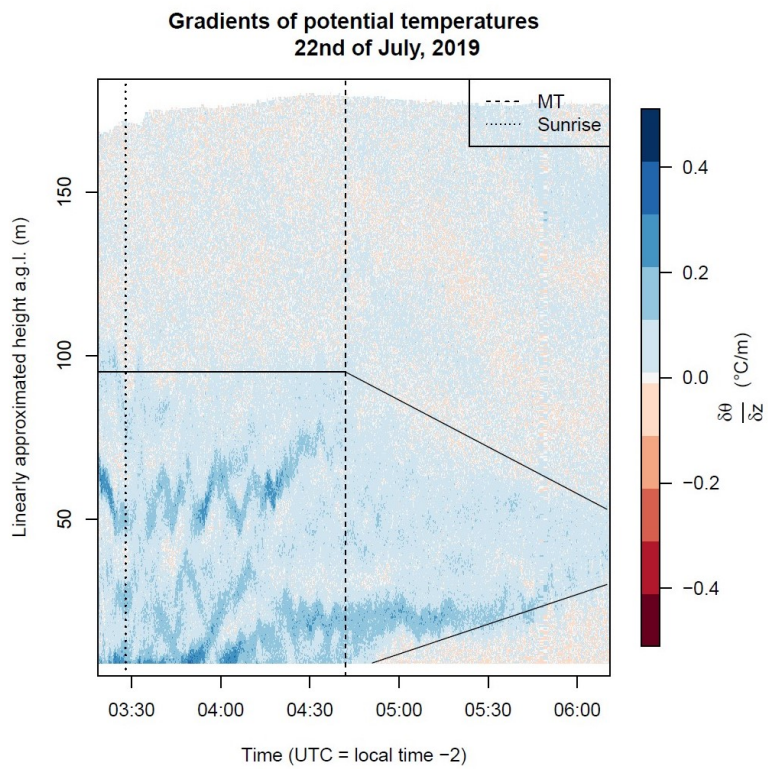


Figure 25: $\frac{\delta\theta}{\delta z}$ -profile of the 22nd of July, sunrise (dotted line), MT (dashed line) and SBL boundaries (solid line)

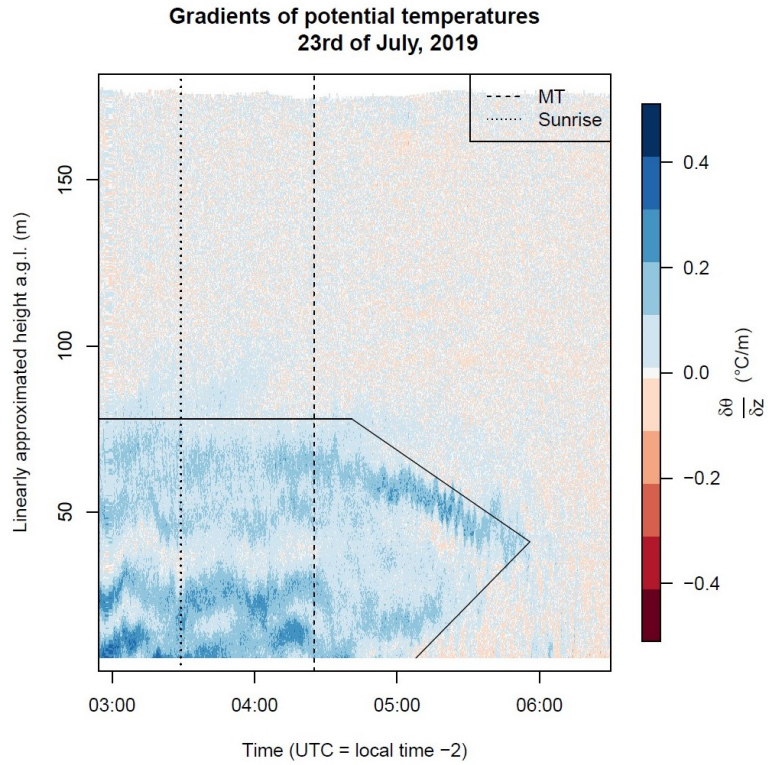


Figure 26: $\frac{\delta\theta}{\delta z}$ -profile of the 23rd of July, sunrise (dotted line), MT (dashed line) and SBL boundaries (solid line)

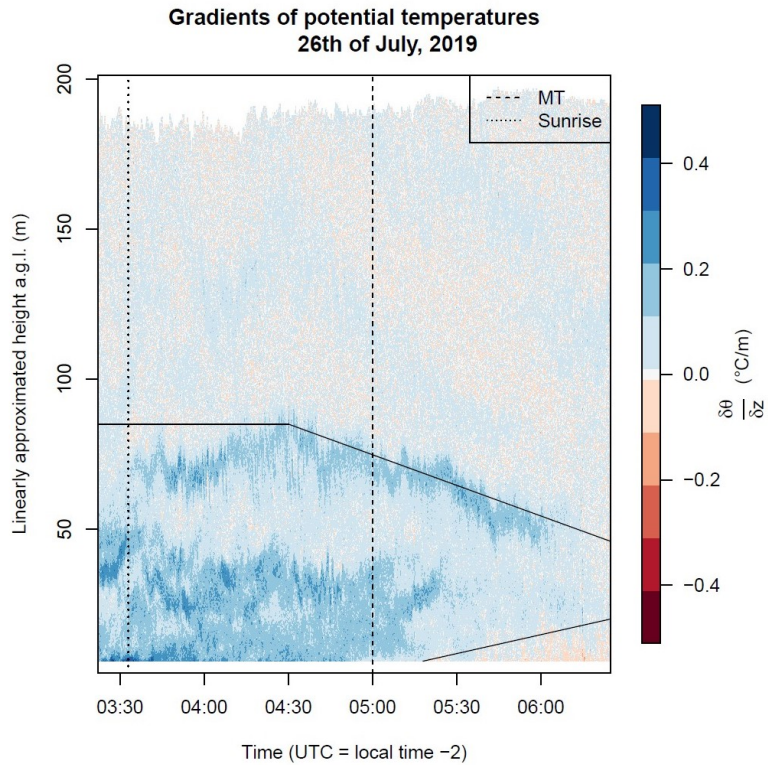


Figure 27: $\frac{\delta\theta}{\delta z}$ -profile of the 26th of July, sunrise (dotted line), MT (dashed line) and SBL boundaries (solid line)

of the boundaries of the SBL, the dashed lines indicate the MT and the dotted lines indicate the sunrise. The expectation was that the MT would occur the same moment as the stability near the surface turns from stable to neutral or unstable. Furthermore, a short delay was expected as the FlyFox profile starts at 6 m a.g.l. due to the calculation of it. Hence, it was expected that the stability would start to turn neutral at the surface and that this change would propagate upwards. By the comparison of the MT and the time when the stability changed, it was found that the MT always occurred before the stability classification changed (Table 3). The time span between the MT in 1.25 m height and the change of the stability in 6 m height varied by a surprising amount between the four observations. Especially these strongly varying time spans show that the MT defined by the direction change of H near the surface isn't always a good indicator for the start of the transformation from the SBL to the MBL. For example, Angevine et al. (2001) defined the morning transition as "the period between sunrise and the time at which the depth of convection reaches about 200 m" [1]. Nevertheless, the FlyFox-V observations reveal that also this definition doesn't perfectly match the process of the transformation. The sun rises far before the transformation occurs (dotted lines, Figure 24 to 27).

To improve it, I propose a new definition of the MT: the MT should be defined as the time span that starts when the thickness of the nocturnal SBL decreases and ends when the stability of the profile doesn't show large stable layers with a spatial extent of at least 2 m any more. To prevent a confusion between these different definitions the newly introduced one will be called Morning Transition Phase (MTP).

This newly introduced MTP now leads to the question of its temporal and spatial scale and the speed of its transformation. The temporal scale is defined as the duration of the MTP and the spatial scale is defined as the interval between the maximum height of the upper boundary and the minimum height of the lower boundary of the SBL. Here, these values could clearly be defined for the flights on the 22nd, the 23rd, and the 26th of July, while the 18th of July shows a very different behavior as will be discussed in Section 6.5.3. In addition to the time and space interval of the MTP, an overall transition velocity is calculated indicating how fast the magnitude of the SBL decreases. For the analyzed days, only the 23rd of July shows a completed transition within the observation period. The other two days have a MTP which exceeds the observation period. Since the calculated transition velocity assumes a completed transition, the transition velocities of days with an incomplete transition are overestimated. For that reason, also changing velocities are calculated which separately quantify the change of the lower and upper boundary of the SBL and only for the period covered by the FlyFox measurement (Table 4).

From Table 4 and Figures 25 to 27, it can be seen that the MTP is a very heterogeneous process with strongly varying temporal and spatial scales. Furthermore, the transformation from a SBL into a MBL isn't only driven from below, but also some processes in the upper regions are important for the change. This process on top of the SBL shows changing velocities of similar magnitude to the changing velocities on the lower boundary, so it cannot be neglected in the study of the SBL evolution. In addition, this appearance of a significant changing velocity of the upper boundary of the SBL supports the need for a definition of the MT which includes a longer process and not only one moment in time that is additionally defined only by surface values.

In summary, all the analysis presented in this section lead to the conclusion that the MT should not only be defined as the first moment when the sensible heat flux near the surface changes its direction. A better approach is to define a MTP which covers the

Overall transition

| Day of Launch | time interval | space interval | transition velocity |
|--------------------------|-----------------|----------------|----------------------|
| 22 nd of July | [04:42 , 06:10] | [0m , 95m] | 0.0184 $\frac{m}{s}$ |
| 23 rd of July | [04:41 , 05:56] | [0m , 78m] | 0.0200 $\frac{m}{s}$ |
| 26 th of July | [04:30 , 06:30] | [0m , 85m] | 0.0118 $\frac{m}{s}$ |

Lower boundary

| Day of Launch | time interval | space interval | changing velocity |
|--------------------------|-----------------|----------------|----------------------|
| 22 nd of July | [04:51 , 06:10] | [6m , 30m] | 0.0051 $\frac{m}{s}$ |
| 23 rd of July | [05:08 , 05:56] | [6m , 41m] | 0.0122 $\frac{m}{s}$ |
| 26 th of July | [05:18 , 06:30] | [6m , 20m] | 0.0032 $\frac{m}{s}$ |

Upper boundary

| Day of Launch | time interval | space interval | changing velocity |
|--------------------------|-----------------|----------------|----------------------|
| 22 nd of July | [04:42 , 06:10] | [53m , 95m] | 0.0081 $\frac{m}{s}$ |
| 23 rd of July | [04:41 , 05:56] | [41m , 78m] | 0.0082 $\frac{m}{s}$ |
| 26 th of July | [04:30 , 06:30] | [46m , 85m] | 0.0054 $\frac{m}{s}$ |

Table 4: Temporal scale, spatial scale, and changing velocities of the transition of the SBL and its boundaries

entire change process from a SBL during the night to a MBL during the day. To make this possible, FlyFox is an extremely powerful method because it sees the changes in gradients with height in a much higher resolution than any conventional instrument. Nevertheless, these conventional instruments are necessary to set the FlyFox observations into a larger context as done in Section 6.5.4.

6.5.3 Morning transition phase on the 18th of July

As pointed out in the previous section, the observations taken at the 18th of July show a very different MTP progression compared to the observations taken on the 22nd, 23rd, and 26th of July. The FlyFox observations don't reveal a well defined MTP as the temperature gradients don't show a strong SBL during the night and no clear change to an entirely mixed layer. For the 22nd, 23rd, and 26th, the SBL shows an "arrow-form": the transformation from the SBL to the MBL starts at the top and the bottom of the SBL and the middle part of the SBL is the last section to turn unstable (compare Figure 25 to 27). In contrast, the SBL of the 18th starts to turn neutral from the middle part and the top is the last part that remains stable (compare Figure 24). This top stable layer additionally shows an upwards movement of about 100 m within about 1.5 h.

Another difference is the air temperatures: during the 18th, clearly lower air temperatures were measured than during the other days (Figures 16 to 19). In addition, the nocturnal temperature gradient over the entire profile is smaller on the 18th than on the 22nd, 23rd, and 26th. Furthermore, the colder temperatures have lead to the occurrence of a 20 m thick fog layer between about 4:00 and 5:30 UTC as they have fallen below the dew point temperature (Figure 28). All these differences between the 18th and the other days may result from the different initial conditions, the fog layer, or a combination of both.

To test whether the initial conditions differ between the four days, the surface parameters mean horizontal wind speed (\bar{U}), turbulent kinetic energy (TKE), sensible heat flux ($w'T'$) and wind direction (ϕ) in 1.25 m height were compared (Figure 29). From



Figure 28: Fog layer on the 18th of July, 2019

these parameters, no difference between the 18th and the other days can be determined. This indicates that the different progression of the MTP can not be explained by the initial condition of local surface parameters. Nevertheless, non-local parameters may have differed between the 18th and the other days.

The fog layer could have influenced the progression of the MTP as the water droplets may have made the fog layer thick for shortwave radiation [4]. This process may have led to a warming of the air right above the fog layer. This warming may then have led to a decreasing stability in the height of the fog layer top due to a positive buoyancy flux. This explanation matches the observed $\frac{\delta\theta}{\delta z}$ -profiles: the air within the fog layer shows a stable stratification (0 to about 25 m, 4:00 to 5:30 UTC, Figure 24) while the air right above it is neutrally or unstable stratified. A second influence which the fog may have had is that it created a surface which was stronger exposed to the incoming shortwave radiation than the ground. By this exposition change, the air mass inside the fog layer may have gained more energy from the incoming shortwave radiation than on a day without fog. When the fog dissolved around 5:30 UTC, this energy was set free and may have led to the quickly increasing instability near the surface (06:00 to end of flight) and the upwards movement of the stable stratified air layer in the top region of the observed profile.

Most likely, the different progression of the MTP on the 18th compared to the other observations was influenced by non-local parameters as well as by the fog.

6.5.4 Bottom-up approach

The high temporal and spatial resolution of FlyFox and its high accuracy does not only enable the investigation of the MTP but also the detection of internal layers and their evolution. In the following section the focus lays on the question whether or not the movement of these layers is initiated from below.

The analysis is conducted on a case study for three internal layers on the 22nd of July (Figure 30). It seems that Layer 1 moves upwards when Layer 2 appears at the bottom of the profile and equally that Layer 2 moves upwards when Layer 3 appears at the bottom of the profile. Even though it is not clear whether Layer 1 or 2, respectively, actually change

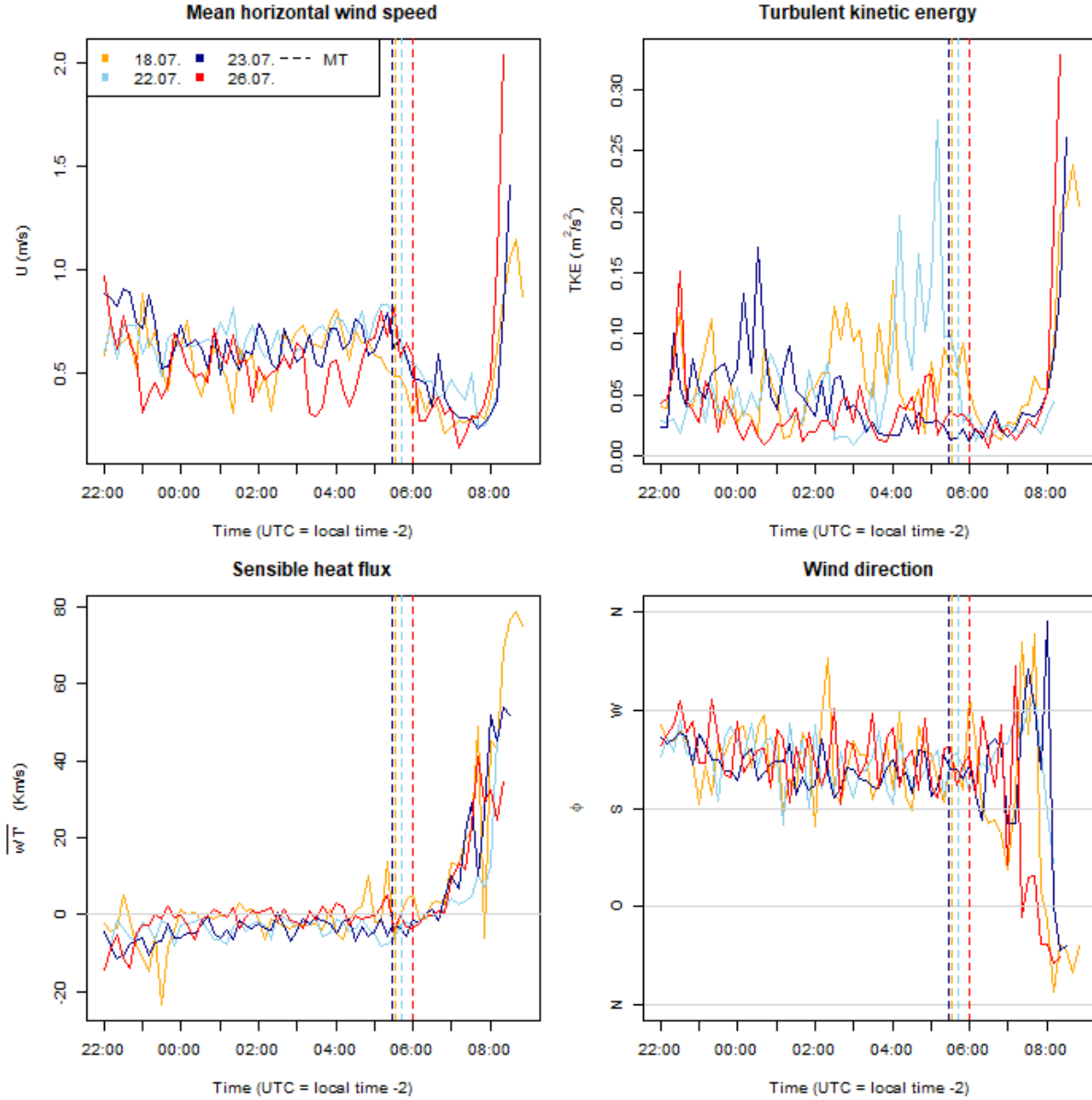


Figure 29: Comparison of initial conditions for all morning transitions

their position or whether only the gradients change in different heights, this phenomenon will be called a movement to simplify the reading of the following analysis.

The hypothesis was that the observed movement of the three internal layers is driven by processes taking place at the surface. From this, it is expected that the data gained by the CSATs in 0.5, 1.25, 4, and 12 m height show similar features and that there is a time lag between a feature appearing in 0.5 m and the same feature appearing in greater heights. Furthermore, it is expected that similar features appear during the strong stable stratification (Layer 1, 3) while different features appear during the weaker stable stratification (Layer 2).

By analyzing the parameters mean horizontal wind speed, mean vertical wind speed, standard deviation (SD) of vertical wind speed (Figure 31), sonic temperature, buoyancy flux, and momentum flux (Figure 32), it is found that the first expectation isn't fulfilled for the observed time interval. The CSATs do not show the same features in all four heights but rather show similar features in the lowest 0.5 to 4 m while different features

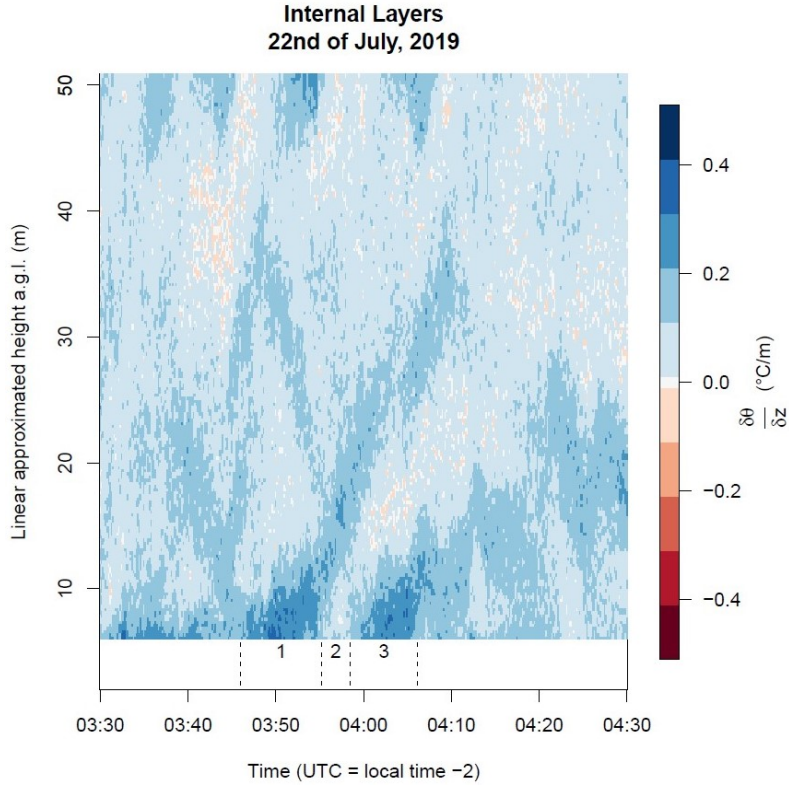


Figure 30: Visualization of the Internal Layers 1, 2, and 3

appear in 12 m height. This indicates that the CSATs in 0.5 and 1 m are located within one internal layer which interacts relatively close with the layer the CSAT in 4 m height is located in. Nevertheless, these lower two layers don't seem to be connected to the layer the CSAT in 12 m height is located in. This shows that a decoupling of the processes in greater heights from the processes near the surface occurs. Hence, a bottom up approach can not explain the movement of the Layers 1, 2 and 3 because no connection between the surface and these layers is given.

Another possible explanation for the occurrence of the three inner layers and their temporal change is the advection of different air masses. The wind directions also measured by the CSATs show a clearly pronounced meandering event before and during the appearance of the three layers (Figure 33). During Layer 1 the air is mainly advected from west. During Layer 2 this direction changes to south or south-west and during Layer 3 it changes again to more west or south-west winds. This direction change is visible in all heights even though it's not equally strong. Air that is advected from the west comes from a relatively flat terrain while air from the south-west comes from the mountain Hohe Heide (224 m higher than experimental site) and air from south comes from the mountain Schneeberg (427 m higher than experimental site). This different source region could explain the difference in the stability of the layers.

Summarizing it, the appearance of the internal layers cannot be explained by a bottom-up approach because the surface layer and the layers above are decoupled from each other. The internal layers can rather be explained by the different source regions of the advected air.

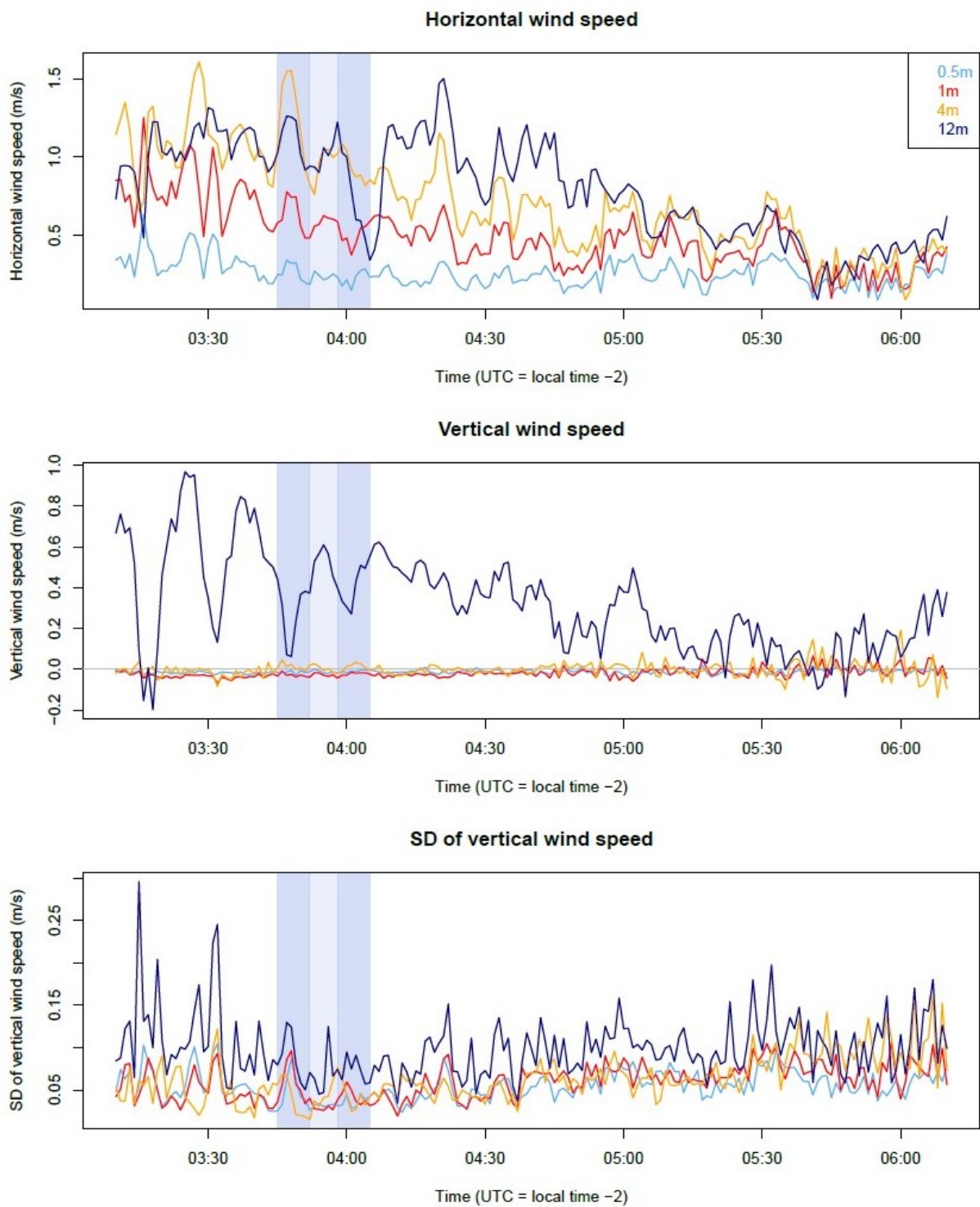


Figure 31: CSAT wind speed data with highlighted strong stable layers (darkblue) and weak stable layer (lightblue), 22nd of July

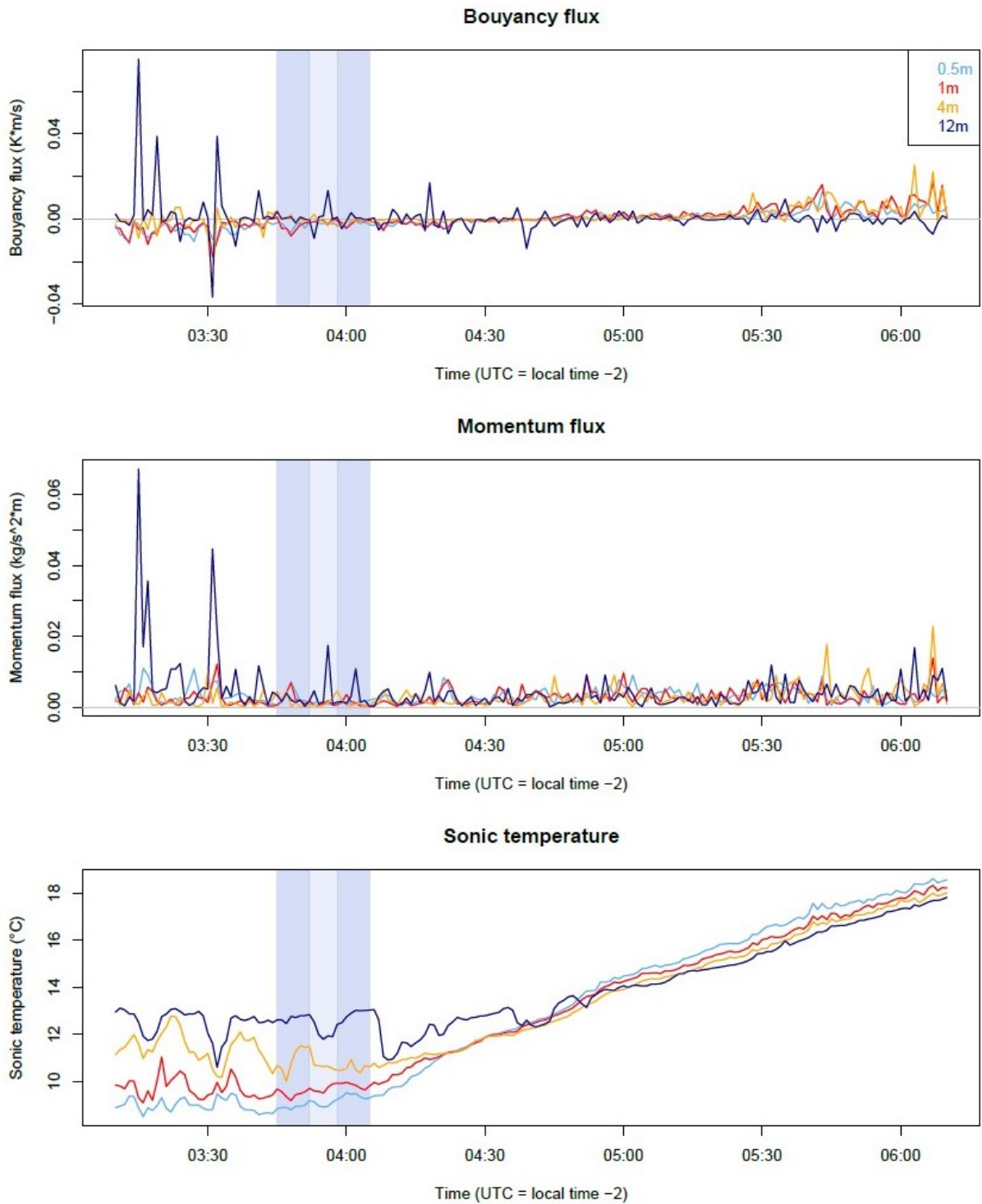


Figure 32: CSAT flux and temperature data with highlighted strong stable layers (dark-blue) and weak stable layer (lightblue), 22nd of July

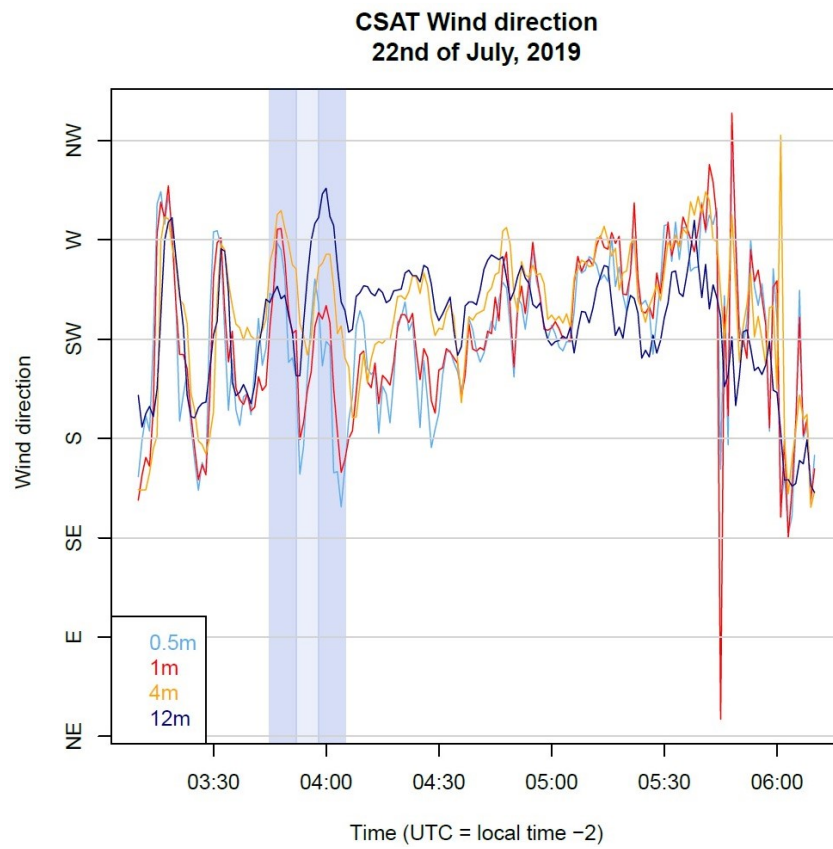


Figure 33: Wind direction for the 22nd of July with highlighted strong stable layers (darkblue) and weak stable layer (lightblue)

7 Conclusion

The overarching goal of this research was to investigate the lower atmospheric boundary layer and to connect it to the surface observations of the LOVE project. As the FlyFox is a new technique, two methodological topics had to be pursued before the actual research questions could be answered:

- First, the movement of the balloon was set into the context of the appearing meteorological conditions. It was found that the balloon mainly responds to horizontal wind speeds and lowers by about 3 m when horizontal wind speeds increase by $1 \frac{m}{s}$.
- Second, each measurement along the optical fiber had to be provided with a height. The comparison of the three height approximations (linear, parabolic, and catenary) showed that the linear height approximation worked best for the very weak wind conditions ($U \leq 1 \frac{m}{s}$) while the parabolic height approximation worked best for the windier conditions ($U > 1 \frac{m}{s}$). Nevertheless, it was found that for the research questions posed in this thesis the linear approximation was sufficient for all conditions since the height error resulting from it did not influence the stability classification needed to answer the research questions.

For the observation of the lower atmospheric boundary layer, two main conclusions can be taken:

- The morning transition which aims to describe the transformation from a nocturnal SBL to a daytime MBL cannot be defined by the direction change of the surface sensible heat flux but needs to be defined as a morning transition phase. This morning transition phase shows a highly varying temporal and spatial scale. The transformation of the SBL to a MBL occurs at the top and the bottom boundary of the SBL simultaneously and with a comparable changing velocity.
- On the 22nd of July, the movement of internal layers of the SBL cannot be explained by a bottom-up approach different internal layers occur within the lowest 12 m which are decoupled from each other. Advection may be a better explanation for it.

These results show that the FlyFox experiment gives great insights into the lower ABL at a high temporal and spatial resolution which aren't possible with traditional instruments. Even though it is limited to weak wind conditions, the MT could be investigated very well. Further work could use it to investigate the late afternoon transition as the MT's counterpart which describes the change from the MBL to the SBL in the evening. It would be interesting whether the late afternoon transition occurs at similar temporal and spatial scales as the morning transition phase.

References

- [1] Wayne M Angevine, Henk Klein Baltink, and Fred C Bosveld. Convective boundary layer. Boundary-Layer Meteorology, 101:209–227, 2001.
- [2] G Ketzler. The Diurnal Temperature Cycle and Its Relation to Boundary-Layer Structure During the Morning Transition. Boundary-Layer Meteorology, 151:335–351, 2014.
- [3] A. Lapworth. The morning transition of the nocturnal boundary layer. Boundary-Layer Meteorology, 119:501–526, 2006.
- [4] B Maronga and F Bosveld. Key parameters for the life cycle of nocturnal radiation fog : a comprehensive large-eddy simulation study. Quarterly Journal of the Royal Meteorological Society, 143:2463–2480, 2017.
- [5] Metek GmbH. RASS 1290 MHz Extension for SODAR PCS . 2000. Technical report, Metek, Elmshorn, Germany, 2014.
- [6] Lena Pfister, Karl Lapo, Chadi Sayde, John Selker, Larry Mahrt, and Christoph K Thomas. Classifying the nocturnal atmospheric boundary layer into temperature and flow regimes. Quarterly Journal of the Royal Meteorological Society, 145:1515–1534, 2019.
- [7] Roland Stull. Practical Meteorology: An Algebra-based Survey of Atmospheric Science. University of British Columbia, 2017.
- [8] Roland B. Stull. An Introduction to Boundary Layer Meteorology. Springer Netherlands, Dordrecht, 6. edition, 1999.
- [9] G. I. Taylor. The spectrum of turbulence. Proceedings of the Royal Society of London. Series A - Mathematical and Physical Sciences, 164:476–490, 1938.
- [10] Christoph Thomas and John Selker. Optical fiber-based distributed sensing methods. unpublished, 2019.

A List of Material

Table 5: Material FlyFox-V

| Material | Explanation |
|----------------------------------|---|
| Balloon | |
| Winch | |
| Winch operator | Make sure this is waterproof |
| Pallet | To fix the winch on it |
| Stones | To put more weight onto the pallet |
| Gas Bottles: He, pressurized air | |
| 2 Pressure regulators | One for Helium; one for pressurized air |
| Hose | To connect the balloon to the gas bottles |
| Strong Net | To fix the Balloon on the ground |
| Rope | To fix the Balloon on the ground + as a connection between the sand bucket and the climbing-carabiner |
| 10 Earth nails | To fix the net / rope on the ground |
| Shackle | To fix the Balloon on one earth nail directly |
| Canvas | To put under the Balloon |
| Safety deflation device | To open the Balloon if it flies away |
| Tether | |
| (Twisted pair) fiber | Spooled in a way so both ends are accessible |
| Empty spool | To wrap the tether around it when the Balloon is at its flying height |
| Fiber roll | To lead the fiber around on top |
| Wormies | To connect the fiber to the tether (upmost: ca. 0.5 m from fiber connection; others: every 50 m) |
| 2 Waterbathes | As reference bathes |
| Aquarium heater | For the warm bath |
| 2 Aquarium pumps | To prevent temperature gradients within the bath |
| 2 Thermometers | To measure the temperature within the bathes (e.g. RBRsolo ³) |
| 2 Strong 12 V batteries | For the winch |
| 10 kg Sand in a bucket | As a weight while carrying the Balloon around |
| 1 Big climbing-carabiner | To connect the sand bucket to the Balloon |
| 2 Smaller carabiners | To fix the reference sensor and the fiber to the tether |
| “Fish scales” | To measure the uplift of the Balloon |
| Balloon repairing kit | |
| Tether sonde | To measure wind speed, temperature and pressure + needs to be fixed on a wind vane |
| Data logger for tether sonde | e.g. Raspberry Pi |
| Computer | To start the Raspberry Pi from |
| Receiver sonde | |
| Laptop | Connected to the receiver sonde to check the pressure while launching |
| DTS Device | |

Table 5: Material FlyFox-V - continuation

| Material | Explanation |
|-----------------------------------|--|
| 6 "Pigtails" (= fiber connectors) | To connect the fiber to the DTS Device and to the connecting fiber |
| One-click device | To clean the pigtails before connecting |
| 2 pair of cloves | |

B FlyFox-V Check-lists

B.1 Refill Check-list

If you're doing a morning flight – do this the evening before!

- Is the balloon properly fixed to the ground?
 - Sand bucket connected? Ground nails fixed? Net ok?
- Check the pressure
 - Push at one of its fins: you should be able to slightly push it in but you should not easily be able to push in all the way to the main "body"
- Refill the balloon
 - Get the hose and the screw-wrench from the metal FlyFox-Box in the back of the trailer
 - Check that the valve at the bottom of the pressure regulator is unscrewed entirely (= closed)
 - Connect pressure regulator to the Helium gas bottle
 - Connect hose to the balloon
 - * Unscrew the golden thing at the end of the hose and screw it onto the balloon
 - * Then connect the hose by screwing the smaller golden thing onto it (otherwise you would have to turn the hose itself which doesn't work)
 - Open all 4 valves starting at the gas bottle
 - * The pressure regulator is broken! Do not wonder if it does weird sounds even if they're quite loud...
 - * Open the valve at the gas bottle very slowly and verify at the balloon that the Helium isn't coming too fast (by sound)
 - Close all 4 valves (starting at the balloon's side) and disconnect the hose

B.2 Preparation Check-list

If you're doing a morning flight – do this the evening before!

- Check the balloon's pressure – if needed follow instructions on the Refill Check-list.
- Check the two calibration bathes
 - 1 working pump per bath
 - 1 heater in the warm bath
- Download the program Arduino IDE on a laptop from Arduino.cc → Software → Downloads
 - make sure this laptop is not needed anywhere else during the flight!
- Start a new Documentation form for the flight
- Prepare the tether sonde
 - Put the wind vane together and tape it onto the sonde (with electric tape)

If you're doing a morning flight – do this in the morning!

- Material needed at the starting area:
 - Take the whole Paper-Box from inside the metal FlyFox-Box with you!
This should include:
 - * 5 wormies
 - * Cloves for 2 people
 - * Tether sonde
 - * One-click device for cleaning the fiber endings
 - * 1 earth nail
 - * Receiver-sonde, connection-cable, laptop
 - * Documentation form, pen
 - * Camping chair to put the winch operator on
 - * Electric tape
 - Take the winch operator (white box) with you.
- Prepare winch
 - Connect the winch operator to the batteries and to the winch itself
 - Make sure the joystick is in a neutral position
 - Choose: Physics → Winder → Joystick
- Start tether sonde
 - Switch the sonde on by plugging in the batteries (only open the lid, you don't need to take the device out of its casing!)
- Prepare the laptop at the launching area

- Connect the Receiver-sonde to the laptop using the cable which is in the same small plastic bag
- Open the program Arduino IDE
- Click on the magnifier in the up-right corner
 - * A new window opens which shows you all received data
 - * The pressure is the signal on Channel 3 received in dPa
- Start the Raspberry Pi to log the tether sonde data
 - Log into the computer at the back of the trailer using Dark\$lab0
 - Open the terminal:

| Text to type in | Explanation |
|--|---|
| ssh pi@132.180.116.135 Password: raspberrry | This accesses the Paspberry Pi |
| Pwd | This tells you the present working directory. It should be /home/pi. |
| sudo su | This makes you a super user |
| sudo rm p[1-4].csv | Deletes the old files p1 – p4. Make sure to double-check that the data has been saved before! |
| ./run.py & | Starts the python script that records the data from the tether sonde in the background. |
 - Open Safari
 - * search for the URL: 132.180.116.135
 - Password: bayeos
 - * Open the Plots and visualize only the pressure data
 - make sure it logs data every second
 - Write down the ground pressure in the Documentation form
 - * Place the Raspberry Pi on top of the trailer
- Switch on deflation device (= little box on the bottom of the balloon)
 - Check the little white valves (bottom left): up – up – up – down (= 900 hPa)
 - Check the lights above the white valves:
 - * two green blinking lights = perfect
 - * orange light = okay but make sure you replace the batteries after the flight
 - * red light = don't fly! Replace the battery with the red light with a new one from the Paper-Box!

B.3 Launching Check-list

- Carry the balloon to the starting area (hold the balloon directly, keep the sand bucket connected)
- Connect the balloon to the winch
 - Use the carabiner and close it properly before disconnecting the sand bucket
- Higher the balloon slowly

– 1st person

- * handle the joystick and constantly check the pressure signal
- * Stop the winch at the following positions by putting the metal stick into the hole in the spool without the tether:

| Position | What to do |
|---------------|--|
| 1st carabiner | Connect the tether sonde |
| 2nd carabiner | Connect the role of the fiber Connect one wormy short behind the green tape |
| P0 – 5 hPa | Connect wormy |
| P0 – 10 hPa | Connect wormy |
| P0 – 15 hPa | Connect wormy |
| P0 – 20 hPa | Fix the balloon (as described below) |

P0 = ground pressure

- * Remember to take out the stick before you start the winch again!

– 2nd person

- * Unroll the fiber so there's no tension on it

- Fix the balloon at its flying height
 - Wrap tether around the black spool (4 – 5 times)
 - Wrap fiber around the black spool (3 times) without any tension on it
 - Place spool in the main wind direction and fix it on the pallet and with the earth nail
- Prepare the bathes
 - Put the fiber from the little spool in 5 “eights” around the structure in the bathes:
 - * first the cold, second the warm bath (as color-coded on the fiber)
 - * make sure the coloured sections stay close the outlet of the bath
 - Make sure to lead the fiber through the outlet at the right side of the lid
- Connect the fiber
 - Clean the pig tails with the one-click
 - Connect the pig tails of the fiber to the ones coming from the trailer → mind the colour-code on it!

- Start the XT
 - Open the XT Client UI at the ToughBook → Configure → load file *LOVE_outer_array_Flyfox_190715* → Edit → Select Channel 4 → Do a test measurement
 - Use Next to navigate through the configuration file → Check all information
 - Select All Channels → Adjust the name of the configuration file to the current date → Save
- Write down the file name, the starting time and all configuration information on the Documentation form
- Make sure to not close the door of the trailer as the Raspberry Pi is on the roof!

B.4 Take down Check-list

- Attach an ice pack at the lowest point of the profile
 - Keep it there for about a minute
 - Write down the time you did this
- Stop the XT
 - Open the XT Client UI at the ToughBook
 - Click Configure → load file → *LOVE_outer_array_190715* → edit
 - Select All Channels → Save
 - Write down the end time on the Documentation form
- Disconnect the bathes and roll up the fiber on the little spool
 - Fix the pig tails on the spool with electric tape
 - Make sure you close the pig tails with the white lits
- Lower the balloon
 - 1st person
 - * Unwind the fiber from the black spool
 - * Unwind the tether from the black spool
 - * Handle the winch and give a countdown as a wormy etc. comes close to it
 - * Stop the tether with the metal stick
 - * Remove the wormies, the fiber and the tether sonde
 - 2nd person
 - * roll up the fiber
 - * keep the fiber straight without putting tension on it
- Connect sand bucket to the balloon as soon as possible
- Bring the balloon back to the trailer and fix it on the ground
 - Keep sand bucket connected
 - Connect the balloon with the shackle directly to the earth nail
 - Put net around it and fix it on the ground
 - Switch off deflation device
 - * Check batterie-lights: if not green, charge/replace the batteries!
- Stop the Raspberry Pi
 - Open the finder and go to */Volumes/darkmix_fieldvault/dm_LOVE2019/Flyfox*
 - * Create a new folder *Launch_1907...* including the current date
 - * Open the new folder and create a folder “Tethersonde”
 - * Copy the pathname of this last folder (right click → command → copy “Tethersonde” as path)

- Open the terminal:

| Text to type in | Explanation |
|--|---|
| exit | Terminates the ssh process |
| sudo killall run.py | Ends the python program |
| ps aux grep python | Asks whether there is still a python program running → should say no! |
| Sftp pi@132.180.116.135 Password: raspberry | Connects to the Raspberry Pi |
| get p4.csv <paste “Tether-sonde” path> | Copies the file p4.csv to the location you created before |

- Go back to the finder and check whether your data is saved there now (this can take a few seconds)
 - * If so, end the sftp connection by typing “bye” into the terminal
- Rename the p4.csv file into *p4_1907..._all.csv*
- Put the Raspberry Pi back into the trailer
- Clean up your working place
 - Make sure all material listed on the “Preparation” Check-list goes back in the metal FlyFox-Box
 - Disconnect the winch operator and bring it back to the trailer
 - * Make sure the connections at the winch are closed
 - Cover up the winch with the green plastic bag and fix it with the strap
 - Put the fiber, the black spool and the Rollprofi next to the bathes
 - Take all electric connections off the ground (e.g. onto the bathes)
- Fill out all missing parts of the Documentation form and hand it to Toni

C Documentation forms

LOVE, FLYFOX-V: Experimental Setup

| | | |
|---|--|-----------------------------------|
| Name(s) of operator(s) | Toni, Anita, Flo | |
| Name of configuration file | LOVE_simba_south_rim_190716 | |
| Instrument, Channel number | Ultima, 3 | |
| Site description | Whale's cove | |
| Date | 18.07.21019 | |
| Time of measurements (UTC) | Start: 05:08 | End: 8:54 |
| Configuration | <input type="checkbox"/> single-ended | <input type="checkbox"/> duplexed |
| Additional remarks | 1s averages every 3s | |
| Boundary layer profile | | |
| Location on fiber (m laf*) | Start: 950 m | End: |
| Time of icepack attach | 8:48 – 8:50 | |
| Tether sonde below balloon | | |
| Name of tether sonde file | | |
| Number of tethersondes used | 1 (top) | |
| Distance of sonde to fiber top (m) | 1.62m | |
| Height at start/end time (m agl) | Start: 0 m | End: 199 m |
| Pressure (hPa) | Ground: 943.4 hPa | Top: 923.5 hPa |
| Fixations for fiber-optic cable to tether (Wormies) | | |
| Number | 4 | |
| Height of fixations (m agl) | Upmost: | Lowest: |
| Cold bath | | |
| Temperature at start/end time (°C) | Start: | End: |
| Location (m laf) | Start: 154.4 m | End: + 4 m |
| Location (m laf) | Start: 2158 m | End: + 4 m |
| Warm bath | | |
| Temperature at start/end time (°C) | Start: | End: |
| Location (m laf) | Start: 146.4 m | End: + 4 m |
| Location (m laf) | Start: 2168.8 m | End: + 4 m |
| Additional measurements | | |
| <input type="checkbox"/> RBRs switched on | <input type="checkbox"/> XT time checked & synchronized | |
| <input type="checkbox"/> Optical connectors cleaned (m/f) | <input type="checkbox"/> Calibration bath pumps & heater running | |
| <input type="checkbox"/> Raspberry Pi logging | | |
| Additional remarks (e.g. weather, calibration, optical connectors) | | |
| New Helium put into Balu | | |
| Cloudless sky | | |
| Meandering in 200 m height (5:40 am; Video taken with field camera) | | |
| Tether sonde data saved with Toughbook instead if DarkMix put computer | | |
| Measured angle (tether to vertical; 5:45 am): 27.6° == 25.7 m height difference | | |
| => max. flight height in the end (no wind): 225.7 m | | |
| Low level jet before sunrise assumed | | |

*laf = length along fiber; agl = above ground level, asl = above sea level

Figure 34: Flight sheet of the 18.07.2019

LOVE, FLYFOX-V: Experimental Setup

| | | |
|---|--|-----------------------------------|
| Name(s) of operator(s) | Toni, Karl | |
| Name of configuration file | LOVE_outer_array_FLYFOX_190722 | |
| Instrument, Channel number | XT, 4 | |
| Site description | Whale's cove | |
| Date | 22.07.21019 | |
| Time of measurements (UTC) | Start: 05:18 | End: 8:10 |
| Configuration | <input type="checkbox"/> single-ended | <input type="checkbox"/> duplexed |
| Additional remarks | 5s averages every 10s | |
| Boundary layer profile | | |
| Location on fiber (m laf*) | Start: 975.145 | End: 1343.73 |
| Time of icepack attach | | |
| Tether sonde below balloon | | |
| Name of tether sonde file | p4_190722_all.csv | |
| Number of tethersondes used | 1 (top) | |
| Distance of sonde to fiber top (m) | 1.62m | |
| Height at start/end time (m agl) | Start: 0 m | End: 199 m |
| Pressure (hPa) | Ground: 953.4 hPa | Top: 933.5 hPa |
| Fixations for fiber-optic cable to tether (Wormies) | | |
| Number | 4 | |
| Height of fixations (m agl) | Upmost: ca. 195 m | Lowest: ca. 50 m |
| Cold bath | | |
| Temperature at start/end time (°C) | Start: | End: |
| Location (m laf) | Start: 154.336 m | End: + 4.07 m |
| Location (m laf) | Start: 2158 m | End: + 4.07 m |
| Warm bath | | |
| Temperature at start/end time (°C) | Start: | End: |
| Location (m laf) | Start: 146.42 m | End: + 4.07 m |
| Location (m laf) | Start: 2168.83 m | End: + 4.07 m |
| Additional measurements | | |
| <input type="checkbox"/> RBRs switched on | <input type="checkbox"/> XT time checked & synchronized | |
| <input type="checkbox"/> Optical connectors cleaned (m/f) | <input type="checkbox"/> Calibration bath pumps & heater running | |
| <input type="checkbox"/> Raspberry Pi logging | | |
| Additional remarks (e.g. weather, calibration, optical connectors) | | |
| Cloudless sky No wind at all No fog but dew formation Super stable layer | | |

*laf = length along fiber; agl = above ground level, asl = above sea level

Figure 35: Flight sheet of the 22.07.2019

LOVE, FLYFOX-V: Experimental Setup

| | | |
|---|--|-----------------------------------|
| Name(s) of operator(s) | Toni, Andreas | |
| Name of configuration file | LOVE_outer_array_FLYFOX_190723 | |
| Instrument, Channel number | XT, 4 | |
| Site description | Whale's cove | |
| Date | 23.07.21019 | |
| Time of measurements (UTC) | Start: 04:59 | End: 8:30 |
| Configuration | <input type="checkbox"/> single-ended | <input type="checkbox"/> duplexed |
| Additional remarks | 5s averages every 10s | |
| Boundary layer profile | | |
| Location on fiber (m laf*) | Start: 978.045 | End: 1340.9 |
| Time of icepack attach | 5:02 | |
| Tether sonde below balloon | | |
| Name of tether sonde file | p4_190723_all.csv | |
| Number of tethersondes used | 1 (top) | |
| Distance of sonde to fiber top (m) | 1.62m | |
| Height at start/end time (m agl) | Start: 0 m | End: 199 m |
| Pressure (hPa) | Ground: 953.4 hPa | Top: 933.5 hPa |
| Fixations for fiber-optic cable to tether (Wormies) | | |
| Number | 4 | |
| Height of fixations (m agl) | Upmost: ca. 195 m | Lowest: ca. 50 m |
| Cold bath | | |
| Temperature at start/end time (°C) | Start: | End: |
| Location (m laf) | Start: 154.336 m | End: + 4.07 m |
| Location (m laf) | Start: 2158 m | End: + 4.07 m |
| Warm bath | | |
| Temperature at start/end time (°C) | Start: | End: |
| Location (m laf) | Start: 146.42 m | End: + 4.07 m |
| Location (m laf) | Start: 2168.83 m | End: + 4.07 m |
| Additional measurements | | |
| <input type="checkbox"/> RBRs switched on | <input type="checkbox"/> XT time checked & synchronized | |
| <input type="checkbox"/> Optical connectors cleaned (m/f) | <input type="checkbox"/> Calibration bath pumps & heater running | |
| <input type="checkbox"/> Raspberry Pi logging | | |
| Additional remarks (e.g. weather, calibration, optical connectors) | | |
| Cloudless sky No wind at all Little meandering at the beginning of the flight North wind (extremely slow) at the end of the flight | | |

*laf = length along fiber; agl = above ground level, asl = above sea level

Figure 36: Flight sheet of the 23.07.2019

LOVE, FLYFOX-V: Experimental Setup

| | | |
|--|--|-----------------------------------|
| Name(s) of operator(s) | Toni, Nico | |
| Name of configuration file | LOVE_outer_array_FLYFOX_190726 | |
| Instrument, Channel number | XT, 4 | |
| Site description | Whale's cove | |
| Date | 26.07.21019 | |
| Time of measurements (UTC) | Start: 05:21 | End: 08:24 |
| Configuration | <input type="checkbox"/> single-ended | <input type="checkbox"/> duplexed |
| Additional remarks | 5s averages every 10s | |
| Boundary layer profile | | |
| Location on fiber (m laf*) | Start: 959.131 m | End: 1359.75 m |
| Time of icepack attach | 5:33 | |
| Tether sonde below balloon | | |
| Name of tether sonde file | p4_190726_all.csv | |
| Number of tethersondes used | 1 (top) | |
| Distance of sonde to fiber top (m) | 1.62m | |
| Height at start/end time (m agl) | Start: 0 m | End: 209 m |
| Pressure (hPa) | Ground: 945.3 hPa | Top: 924.4 hPa |
| Fixations for fiber-optic cable to tether (Wormies) | | |
| Number | 4 | |
| Height of fixations (m agl) | Upmost: ca. 195 m | Lowest: ca. 50 m |
| Cold bath | | |
| Temperature at start/end time (°C) | Start: | End: |
| Location (m laf) | Start: 154.336 m | End: + 4.07 m |
| Location (m laf) | Start: 2158 m | End: + 4.07 m |
| Warm bath | | |
| Temperature at start/end time (°C) | Start: | End: |
| Location (m laf) | Start: 146.42 m | End: + 4.07 m |
| Location (m laf) | Start: 2168.83 m | End: + 4.07 m |
| Additional measurements | | |
| <input type="checkbox"/> RBRs switched on | <input type="checkbox"/> XT time checked & synchronized | |
| <input type="checkbox"/> Optical connectors cleaned (m/f) | <input type="checkbox"/> Calibration bath pumps & heater running | |
| <input type="checkbox"/> Raspberry Pi logging | | |
| Additional remarks (e.g. weather, calibration, optical connectors) | | |
| Cloudless sky Raspberry Pi logs in irregular time steps (only in the beginning) Meandering in the morning at 200m Sun reached the launching area at ca. 6:50 am | | |

*laf = length along fiber; agl = above ground level, asl = above sea level

Figure 37: Flight sheet of the 26.07.2019